Proofs to: Dr. George Britovsek
Department of Chemistry
Imperial College London
Exhibition Road
South Kensington
London SW7 2AY
UK
Tel. +44-(0)20-75945863
Fax. +44-(0)20-75945804
e-mail: g.britovsek@imperial.ac.uk

Towards Robust Alkane Oxidation Catalysts: Electronic Variations in Non-Heme Iron(II) Complexes and their Effect in Catalytic Alkane Oxidation

Jason England, Reema Gondhia, Laura Bigorra-Lopez, Allan R. Petersen, Andrew J.P. White and George J.P. Britovsek*

Department of Chemistry, Imperial College London, Exhibition Road, London, SW7 2AY, UK.

Abstract

A series of non-heme iron(II) bis(triflate) complexes containing linear and tripodal tetradentate ligands has been prepared. Electron withdrawing and electron donating substituents in the *para* position of the pyridine ligands as well the effect of pyrazine *versus* pyridine and sulphur or oxygen donors instead of nitrogen donors have been investigated. The electronic effects induced by these substituents influence the strength of the ligand field. UV-vis spectroscopy and magnetic susceptibility studies have been used to quantify these effects and VT ^{1}H and ^{19}F NMR spectroscopy as well as X-ray diffraction have been used to elucidate structural and geometrical aspects of these complexes. The catalytic properties of the iron(II) complexes as catalysts for the oxidation of cyclohexane with hydrogen peroxide have been evaluated. In the strongly oxidising environment required to oxidise alkanes, catalyst stability determines the overall catalytic efficiency of a given catalyst, which can be related to the ligand field strength and the basicity of the ligand and its propensity to undergo oxidation.

Introduction

The selective oxidation of aliphatic C-H bonds has been a long-standing goal in chemical research.[1-4] Despite several industrial applications such as the oxidation of cyclohexane and p-xylene, which use O_2 as the oxidant and manganese or cobalt based catalysts, the development of practical oxidation catalysts and a thorough mechanistic understanding of alkane oxidation processes continue to provide great challenges in catalysis research. A number of different classes of alkane oxidation catalysts have been developed during the last 50 years, including the cobalt and manganese acetate catalyst systems used industrially,[5] the heme-based iron complexes containing porphyrin-type ligands used in nature,[6, 7] polyoxometalates[8-10] and more recently, non-heme iron based catalyst systems.[11-17] The metal catalysts are typically combined with oxidants, which can have different oxo transfer abilities[18], for example H_2O_2, O_2, ClO^-, PhIO, O_3 or N_2O, whereby the first two oxidants are economically and environmentally the most attractive oxidants.[19, 20]

An appealing feature of non-heme iron catalysts is that ligand modifications and catalyst tuning are relatively straightforward, compared for example with porphyrin-type ligand systems. However, many non-heme iron complexes that have been reported as oxidation catalysts in combination with H_2O_2 have shown catalytic behaviour which is characterised by low conversions (of alkane substrate and H_2O_2) and low product selectivities, either due to catalyst decomposition or extensive H_2O_2 decomposition due to the formation of hydroxyl (OH·) radicals (Fenton chemistry).[21] In contrast, some non-heme iron complexes have shown a dramatically different behaviour. Much higher conversions of H_2O_2 into oxidised products, combined with a more selective oxidation reactivity have been observed with certain non-heme iron(II) complexes containing tetradentate nitrogen-based ligands, which can be classified into the following categories, according to their ligand structure: *tripodal tetradentate ligands* such as TPA[22, 23] and *iso*-BPMEN,[24] *linear tetradentate ligands* such as BPMEN,[25] BQEN [26] and (*S*,*S*-PDP)[27] and *cyclic tetradentate ligands*, for example ^{Me2}PyTACN (see Figure 1).[28, 29]

Several non-heme iron catalysts have shown stereospecific and dioxygen-independent oxidation of alkanes with H_2O_2[13, 17, 30] and the C-H regio-selectivities and kinetic isotope effects have indicated a more selective oxidant than those responsible for oxidation in Fenton-type systems. This different catalyst behaviour in

combination with isotope labelling studies[31] and DFT calculations[32] have implicated a high valent iron(V) oxo species as the active oxidant,[33, 34] which suggests that the reaction mechanism for these non-heme systems could be analogous to the mechanism for heme systems such as Cytochrome P-450,[6] i.e. hydrogen atom abstraction followed by rapid oxygen rebound.[35] Several Fe(IV) oxo complexes have now been isolated and crystallographically characterised and evidence for the existence of iron(V) oxo complexes is mounting.[36-39]

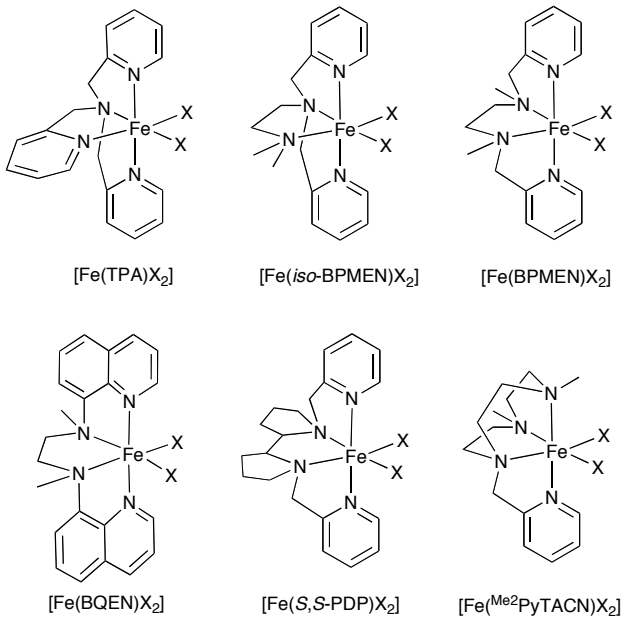

Figure 1. Examples of non-heme iron(II) oxidation catalysts.

Common features in these non-heme iron catalysts are the use of tetradentate ligands with amine or pyridine-type donors and two *cis* labile co-ligands X, for example weakly coordinating triflate anions or acetonitrile molecules in combination with non-coordinating anions. One of the main questions that immediately arises is: Why are these particular catalysts so much better than other classes of non-heme iron(II) complexes? In a series of papers, we and others have addressed this question by systematically investigating the ligand-based requirements that are needed for the formation of efficient oxidation catalysts. For example, steric effects in TPA-type iron(II) catalysts have been investigated by Que and co-workers, by introducing methyl substituents in the pyridyl *ortho* positions.[30, 40, 41] Electronic effects have been investigated by the introduction of nitro substituents in the pyridyl *para* positions.[42] Both variations have led to reduced catalytic activity. Changes to the backbone of

BPMEN and BQEN type ligands have resulted in an increase in ligand flexibility and different coordination modes, generally resulting in lower catalytic activity.[26, 43, 44] As a result of these studies, it has become increasingly clear that catalyst stability, under the harsh oxidising conditions required to oxidise alkanes, is a major factor in determining the catalytic efficiency of a given catalyst. Ligand rigidity and a strong ligand field appear to be critically important for the stability and lifetime of these non-heme catalysts. The endemic but often ignored problem of catalyst degradation, especially in oxidation catalysis, has been investigated previously for several related systems.[45-47] Porphyrin-based iron catalysts have long been known to degrade during oxidation catalysis and, together with increased rates of H_2O_2 decomposition, this has been attributed to higher concentrations of hydroxyl radicals.[48-51] In fact, the problem also exists in living organisms, where heme and non-heme oxidases have a limited lifetime, but nature has developed a sophisticated catalyst regeneration system to overcome this problem.[52]

Here we report our investigations into electronic effects on the catalytic activity of non-heme iron catalysts containing linear and tripodal tetradentate ligands. The aim of this study is to elucidate the ligand-based requirements needed for high catalytic activity in these systems. The different substituents in the *para* position of the pyridine donors are expected to affect catalyst stability and activity. In addition, different bridging donor atoms (sulphur and oxygen) have been introduced to assess the importance of the central amine donors. Three classes of iron(II) complexes have been prepared (see Figure 2) with different substituents at the *para* position of the pyridine donors in BPMEN (class I) and iso-BPMEN ligands (class III). The variations on the bridging amine donors in BPMEN have been investigated by using ether and thioether donors (class II). The coordination geometries of the iron(II) bis(triflate) complexes have been determined in the solid state and in solution. The spectroscopic and magnetic properties of the iron(II) complexes have been measured, in an attempt to correlate the coordination geometry and the ligand field strength with the catalytic activity and selectivity of these complexes for the oxidation of cyclohexane with H_2O_2 as the terminal oxidant.

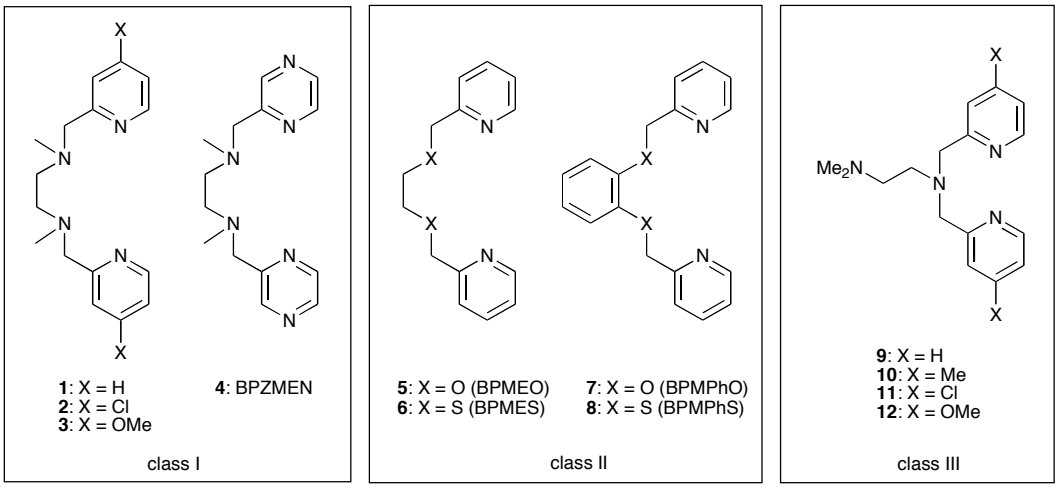

Figure 2. Ligand classes I–III.

Results and Discussion

Synthesis of ligands and complexes

The synthesis of the functionalised BPMEN-type ligands of class I (**1** – **3**) has been reported previously and they have been used as ligands for the preparation of manganese complexes.[24, 53, 54] The bis(pyrazyl) ligand BPZMEN **4** was prepared by methylation of the previously reported precursor.[55]

The preparation of the novel oxygen-bridged ligands **5** and **7** was less straightforward. The reaction between picolyl chloride and ethylene glycol, using a variety of bases and reaction conditions, invariably resulted in a complex mixture of products, probably due to the low nucleophilicity of the alkoxide ion. Ligand **5** was eventually prepared by nucleophilic substitution in DMSO, using NaH as the base. This reaction also led to mixture of compounds, but the desired product BPMEO **5** could be isolated by column chromatography in 24 % yield. In the case of the catechol bridged ligand BPMPhO **7**, phase transfer conditions were employed as described previously for similar compounds.[56] The sulphur bridged ligand BPMES **6** was prepared as reported previously from ethane dithiol and picolyl chloride, using sodium ethoxide as the base,[57] and the novel phenylene bridged ligand **8** was prepared *via* a similar procedure. The *iso*-BPMEN ligand series of class III (**10** – **12**) was prepared *via* reductive amination, in an analogous fashion to our previously reported synthesis of *iso*-BPMEN **9**, using the corresponding *para*-substituted pyridine-2-carboxaldehydes and N,N-(dimethyl)ethylene diamine.[24]

An overview of the most likely structures of the complexes prepared in this study is shown in Figure 3. The preparation of the iron(II) bis(triflate) complexes was generally carried out by mixing THF solutions of the ligand and $Fe(OTf)_2(CH_3CN)_2$ which yielded, upon stirring overnight, the desired complex. Attempts to form the *p*-methyl and *p*-chloro derivatives [Fe(**10**)$(OTf)_2$] and [Fe(**11**)$(OTf)_2$] by this route were unsuccessful, yielding only impure darkly-coloured sticky solids. In contrast, reaction of the ligands **10** and **11** with iron(II) dichloride in THF led upon stirring for 24 hours to precipitation of the complexes [Fe(**10**)Cl_2] and [Fe(**11**)Cl_2]. Reaction of these dichloro complexes with two equivalents of silver(I) triflate gave, after filtration to remove silver chloride, the targeted complexes [Fe(**10**)$(OTf)_2$] and [Fe(**11**)$(OTf)_2$]. All complexes of the type [Fe(L)Cl_2] or [Fe(L)$(OTf)_2$] (L = **1**-**12**) investigated here are paramagnetic high spin iron(II) complexes, both in the solid state and in non-coordinating solvents such as dichloromethane. Dissolution of the complexes [Fe(L)$(OTf)_2$] (L = **1**-**12**) in acetonitrile results in the immediate formation of the bis(acetonitrile) dicationic complex $[Fe(L)(CH_3CN)_2]^{2+}$ as the major species in solution. For some ligands, small amounts (< 5%) of a triflate coordinated complex $[Fe(L)(CH_3CN)(OTf)]^+$ can also be detected by ^{19}F NMR (*vide infra*). Depending on the strength of the ligand field, these iron(II) complexes can be in a temperature-dependant spin crossover regime. The complexes have been characterised by variable temperature ^1H NMR, ^{19}F NMR and magnetic susceptibilities, as well as UV-Vis spectroscopy and in the case of complexes [Fe(**6**)$(OTf)_2$] and [Fe(**7**)$(OTf)_2$] the solid state structures have been determined by X-ray diffraction.

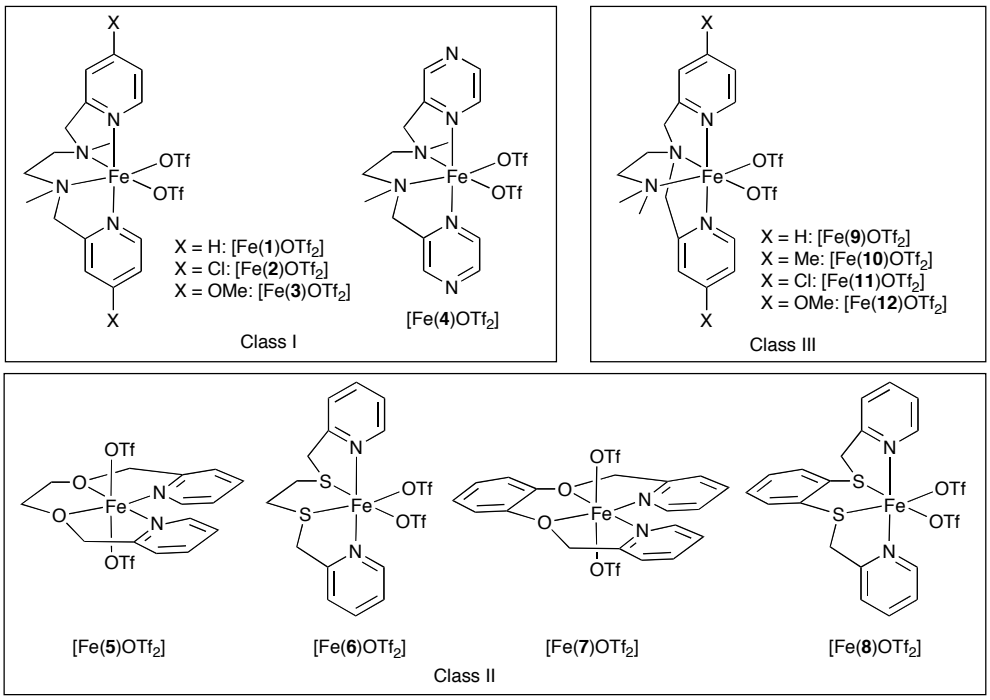

Figure 3. The most likely structures for the iron(II) bis(triflate) complexes of ligands **1**–**12**.

Solid State Structures

Linear tetradentate ligands can adopt three coordination modes in octahedral metal complexes: *cis*-α, *cis*-β and *trans*. The two internal donors become chiral upon coordination to the metal and can therefore have either the same or opposite configuration. Assuming that the configuration of these internal two donors remains unchanged, this increases the number of possible isomers to five pairs of enantiomers: *cis*-α (*R**,*R**), *cis*-β (*R**,*R**) or *cis*-β (*R**,*S**) and *trans* (*R**,*R**) or *trans* (*R**,*S**), whereby *R** and *S** denote the relative configuration at the internal donor atoms.[44] From molecular models it is immediately evident that the *cis*-α (*R**,*S**) geometry is not possible due to severe bite-angle strain within the complex. Whichever geometry a linear tetradentate ligand will adopt preferentially in a metal complex is not easily predicted and depends on a number of factors, including the number of atoms between the donors, the solvent and the temperature. In addition, if the co-ligands are labile such as triflate or acetonitrile ligands, equilibria can exist between the different geometries in solution, which will be concentration and temperature dependent. The coordination geometries observed in the solid state are therefore not necessarily the same as those in solution, as was shown previously for iron(II) complexes containing

bis(pyridylmethyl)diamine and bis(quinolyl)diamine ligands.[26, 44, 58] For the tripodal tetradentate ligands **9**-**12**, only one coordination geometry is possible, and the molecular structures for the ligands **10**-**12** are expected to be the same as the solid state structure determined previously for [Fe(**9**)$(OTf)_2$].[24]

In the case of complexes featuring BPMEN (**1**) or the related ligands **2**-**4** with three 5-membered chelate rings, the *cis*-α (*R**,*R**) geometry with a twist conformation of the central chelate ring is the most likely coordination geometry. This geometry results in the least amount of bite angle strain[59] and is the only geometry seen in solid state structures of related iron(II) complexes.[25, 60-64] The iron(II) bis(triflate) complexes containing the sulfur bridged ligand BPMES **6** will adopt most likely the *cis*-α geometry, as this would result in a similar bite angle strain as for BPMEN and this is the geometry seen in the nickel(II) complex [Ni(**6**)$(CH_3CN)_2]^{2+}$ and the vanadium(IV) complex [V(**6**)(O)(Cl)]$^+$.[65, 66]

X-ray analysis of crystals of [Fe(**6**)OTf_2] revealed the presence of two independent C_2-symmetric complexes (with similar conformations but opposite chiralities) in the asymmetric unit (complex A is shown in Figure 4, complex B in Figure S19 in the Supporting Information). Each complex has the expected *cis*-α (*R**,*R**) geometry, the two pyridyl nitrogen donor atoms occupying sites trans to each other with an N–Fe–N angle of 158.7(4)° [158.8(4)°] (the number in square parentheses refers to complex B). The five-membered S,N chelate ring has an envelope geometry, the sulphur lying ca. 0.36 Å [0.31 Å] out of the {C_2NFe} plane which is coplanar to within ca. 0.02 Å [0.03 Å]. The five-membered S,S' ring, through which the C_2 axis passes, has a twisted geometry with the two carbon atoms lying ca. 0.30 Å [0.35 Å] above and below the {S_2Fe} plane respectively; in complex A this gives the ring a λ twist, whilst complex B has a δ twist. The strain involved in this conformation of the tetradentate S,S',N,N' ligand is shown by the ca. 11° [11°] departure from ideal of the N–Fe–N *trans* angle (*vide supra*) and the ca. 11° [13°] twist between the {FeS_2} and {FeO_2} coordination planes.

A search of the Cambridge Structural Database (version 5.29, Jan-2008 update) for the Fe–S bond lengths in iron thioether complexes (similar to that done by Schmiege et al.,[67] but with a newer version of the database) gave a double-peak

histogram (see Figure S23). The first, much larger, peak is centred at ca. 2.27 Å, which corresponds to the average bond length in Fe(0) and low spin Fe(II) thioether complexes. A second, much smaller peak is centred at ca. 2.56 Å, the typical Fe–S distance for HS Fe(II) and Fe(III) compounds. The Fe–S bond lengths seen here of 2.5180(18) Å and 2.515(3) Å in complexes A and B respectively, together with the long Fe–N bond lengths confirm that [Fe(**6**)OTf_2] is a HS Fe(II) complex in the solid state.

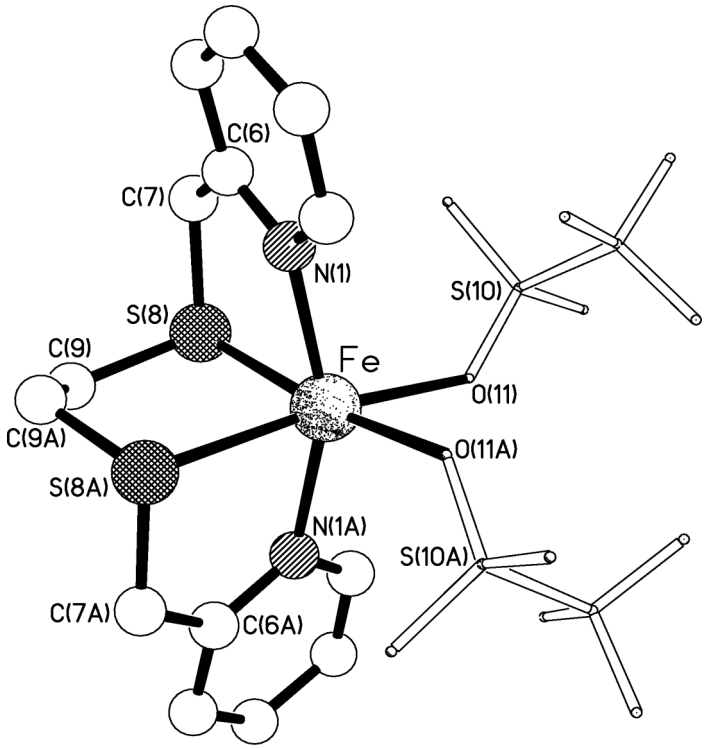

Figure 4. The molecular structure of one (A) of the two crystallographically independent C_2 symmetric complexes present in the crystals of [Fe(**6**)OTf_2]. The atoms labeled with an "A" suffix are related to those without the suffix by the operation of the 2-fold axis that passes through the metal centre and bisects the C(9)–C(9A) bond (-x+2,y,-z+3/2).

We have previously reported that, when the bridging moiety in the BPMEN ligand **1** is changed from an ethylene bridge to a phenylene bridge, the preferred geometry in solution is no longer the *cis*-α(*R**,*R**) geometry, despite this being the geometry observed in the solid state.[44] In dichloromethane solution, in addition to the *cis*-α(*R**,*R**) geometrical isomer (ca. 40%), an inter-converting mixture of the *cis*-

β(*R**,*S**) and the *trans* (*R**,*S**) geometries (ca. 20 and 40%, respectively) was observed by VT ^{19}F NMR spectroscopy.

The solid state structure of the dioxophenylene bridged complex [Fe(**7**)OTf_2] revealed to our surprise a distorted *trans* geometry (see Figure 5), the tetradentate N,N',O,O' ligand having an approximately planar conformation. The atoms of the N(1),O(8) and O(8),O(15) five-membered chelate rings, plus the N(22) donor atom of the O(15),N(22) ring, {Fe,N(1),C(6),C(7),O(8),C(9),C(14),O(15),N(22)}, are coplanar to within ca. 0.06 Å with C(16) and C(17) lying ca. 0.46 and 0.23 Å out of this plane on the same side [towards O(41)]. Whilst the Fe–N and Fe–O(triflate) bonds (Table 2) are roughly comparable to those in complex [Fe(**6**)OTf_2] (Table 1), the change from an SCH_2CH_2S backbone in [Fe(**6**)OTf_2] to the OCH_2CH_2O backbone here in [Fe(**7**)OTf_2] results in a ca. 0.33 Å reduction in the Fe–X bond lengths to these donor atoms. This, combined with the forced planarity of the central O,O' five-membered chelate ring in [Fe(**7**)OTf_2]. c.f. the twisted conformations seen for the C_2S_2Fe ring in [Fe(**6**)OTf_2], appear to be responsible for the change from a *cis*-α (*R**,*R**) to a *trans* conformation. The unusual trigonal planar coordination of the oxygen atoms O(8) and O(15) suggests significant sp^2 hybridisation and precludes assignment of their stereochemical configuration. Associated with this change in conformation from *cis*-α to *trans* is a further distortion from linear for the *trans* N–Fe–N angle, which is 142.72(6)° compared to ca. 159° in [Fe(**6**)OTf_2].

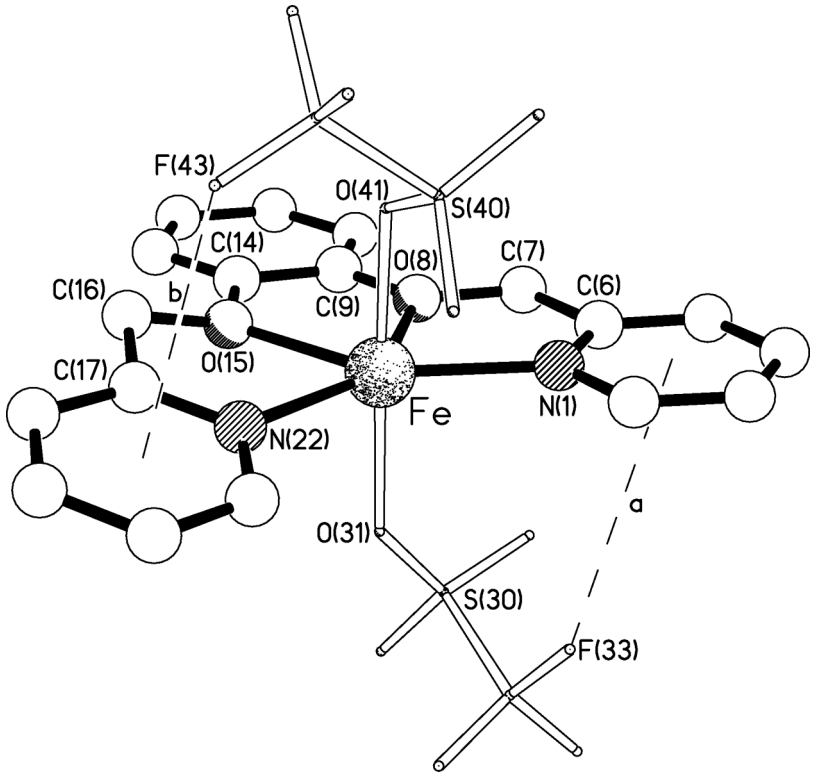

Figure 5. The molecular structure of [Fe(**7**)OTf$_2$]. The F···π separations are (a) 3.71 Å, and (b) 3.32 Å.

Table 1. Selected bond lengths (Å) and angles (°) for both (A and B) of the two crystallographically independent C_2 symmetric complexes present in the crystals of [Fe(**6**)OTf$_2$].[a]

	A	B		A	B
Fe–N(1)	2.183(6)	2.172(8)	Fe–S(8)	2.5180(18)	2.515(3)
Fe–O(11)	2.132(6)	2.114(7)			
N(1)–Fe–S(8)	80.01(17)	79.8(2)	N(1)–Fe– O(11)	103.2(2)	103.8(3)
N(1)–Fe–N(1A)	158.7(4)	158.8(4)	N(1)–Fe–S(8A)	84.55(18)	84.9(2)
N(1)–Fe– O(11A)	92.5(2)	92.2(3)	S(8)–Fe–O(11)	94.50(17)	95.5(2)
S(8)–Fe–S(8A)	87.13(8)	87.48(14)	S(8)–Fe–O(11A)	172.19(15)	171.15(19)
O(11)–Fe–O(11A)	84.9(3)	82.9(4)			

[a] The atoms labeled with an "A" suffix are related to those without the suffix by the operation of the 2-fold axis (-x+2,y,-z+3/2).

Table 2. Selected bond lengths (Å) and angles (°) for [Fe(**7**)OTf$_2$].

Fe–N(1)	2.1542(15)	Fe–O(8)	2.1719(12)
Fe–O(15)	2.2026(12)	Fe–N(22)	2.1342(15)
Fe–O(31)	2.1550(14)	Fe–O(41)	2.1565(14)
N(1)–Fe–O(8)	73.92(5)	N(1)–Fe–O(15)	144.31(5)

N(1)–Fe–N(22)	142.72(6)	N(1)–Fe–O(31)	90.90(5)
N(1)–Fe–O(41)	87.73(6)	O(8)–Fe–O(15)	70.53(5)
O(8)–Fe–N(22)	143.37(5)	O(8)–Fe–O(31)	91.27(5)
O(8)–Fe–O(41)	91.28(5)	O(15)–Fe–N(22)	72.89(5)
O(15)–Fe–O(31)	92.84(5)	O(15)–Fe–O(41)	90.05(5)
N(22)–Fe–O(31)	88.58(6)	N(22)–Fe–O(41)	90.66(6)
O(31)–Fe–O(41)	176.65(5)		

^{1}H-NMR Spectroscopy

Upon dissolution in CD_3CN, the $[Fe(L)(OTf)_2]$ complexes presented here undergo fast substitution reactions to give complexes of the type $[Fe(L)(CD_3CN)_2](OTf)_2$, which can exist in a spin crossover regime.[68] The rapid interconversion between paramagnetic high spin (HS) and diamagnetic low spin (LS) complexes, combined with the exchange of coordinated and free acetonitrile and triflate ligands, results in very broad ^{1}H NMR signals at room temperature, which make the characterisation of these complexes by ^{1}H NMR spectroscopy not straightforward. For example, complex $[Fe(\mathbf{1})(CD_3CN)_2](OTf)_2$ is at higher temperatures (above 330K) exclusively HS and ligand exchange is faster than the NMR timescale, resulting in a paramagnetic spectrum with relatively sharp signals (see Figure 6). At lower temperatures (below 230K), the complex is exclusively LS, resulting in a diamagnetic ^{1}H NMR spectrum. The temperature-dependant ^{1}H NMR behaviour of the related complex $[Fe(\mathbf{1})(CH_3CN)_2][ClO_4]_2$ in CD_3CN solution has been analysed previously.[69] However, the reported peak assignments are not entirely correct. The protons that undergo the largest downfield shift when the temperature is increased (H^{α}, H^{A} and H^{C}) are those with a Fe-N-C-H dihedral angle close to 0 or 180 degrees, because this allows the most efficient spin transfer from the paramagnetic iron centre to the hydrogen atoms.[70] The dihedral angles for the individual protons, determined from the two X-ray crystal structures that are available for the cation $[Fe(\mathbf{1})(CH_3CN)_2]^{2+}$,[25, 64] are given, together with the our peak assignments, in Figure 6. Further evidence was obtained from variable temperature ^{1}H NMR measurements and a NOESY spectrum at 226 K (see Figures S1 and S2). Peak assignments for the related complexes $[Fe(\mathbf{2})(OTf)_2]$ and $[Fe(\mathbf{3})(OTf)_2]$ containing a *para*-chloro and a *para*-methoxy substituent, respectively, were made accordingly (see Figures S3 and S4).

Torsion angle	Degrees
Fe-N-C-H^{α}	0
Fe-N-C-H^{A}	161
Fe-N-C-H^{B}	81
Fe-N-C-H^{C}	162
Fe-N-C-H^{D}	79

Values from ref. 25 and 64

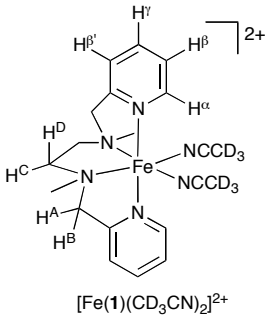

$[Fe(\mathbf{1})(CD_3CN)_2]^{2+}$

Figure 6. ^{1}H NMR spectrum of $[Fe(\mathbf{1})(OTf)_2]$ at 298K in CD_3CN. Torsion angles in complex $[Fe(\mathbf{1})(CH_3CN)_2]^{2+}$ have been determined from the solid state structures reported in references 25 and 64 (* = CH_3CN).

Variable temperature ^{1}H NMR studies have shown that line broadening begins with the onset of the spin-crossover (SC) and becomes increasingly severe with increasing temperature, with the result that at T > 298 K many resonances are not resolved and the ^{1}H NMR spectrum can no longer be assigned. However, at T = 343 K where there is almost complete occupation of the HS configuration, the resonances begin to sharpen. This line-broadening phenomenon is consistent with a fluxional process that is accessed upon initiation of spin-crossover and becomes increasingly faster with increasing temperature.

The LS configuration appears to be accessible only for the dicationic bis(acetonitrile) complexes $[Fe(L)(CH_3CN)_2]^{2+}$, while triflate ligands and 5-coordinate geometries do not exert a sufficiently large ligand field to induce anything other than HS configurations within the temperature range. The inherent stabilisation of the d^6 LS state inhibits dissociation of an acetonitrile ligand and exchange with a triflate

anion, i.e. LS iron(II) complexes are substitutionally inert. Upon thermal initiation of spin-crossover, population of the HS configuration of $[Fe(L)(CH_3CN)_2]^{2+}$ occurs, from which a reduced energetic barrier for substitution leads to the formation of HS triflate coordinated complexes, most likely *via* high-spin 5-coordinate species. These considerations represent a mechanism for fluxional exchange of acetonitrile and triflate ligands initiated by spin crossover. This behaviour is illustrated for complex [Fe(**4**)$(OTf)_2$] containg the BPZMEN ligand.

The ^{1}H-NMR spectrum of complex [Fe(**4**)$(OTf)_2$], dissolved in CD_3CN at 298 K, displays severe line-broadening (Figure S5). Consistent with the low magnetic moment of 2.86 BM at 298 K in CD_3CN solution, the corresponding chemical shift range is small (*ca*. 0-20 ppm, i.e. close to the diamagnetic region). The line-broadening in the ^{1}H-NMR spectrum derives from exchange between coordinated and non-coordinated acetonitrile and triflate ligands. At 238 K, a diamagnetic ^{1}H-NMR spectrum without line-broadening is observed (Figure 7). With increasing temperature, the chemical shift range gradually increases, whereby the protons H^{α}, H^A and H^C experience the largest downfield shift (see Figure S6).

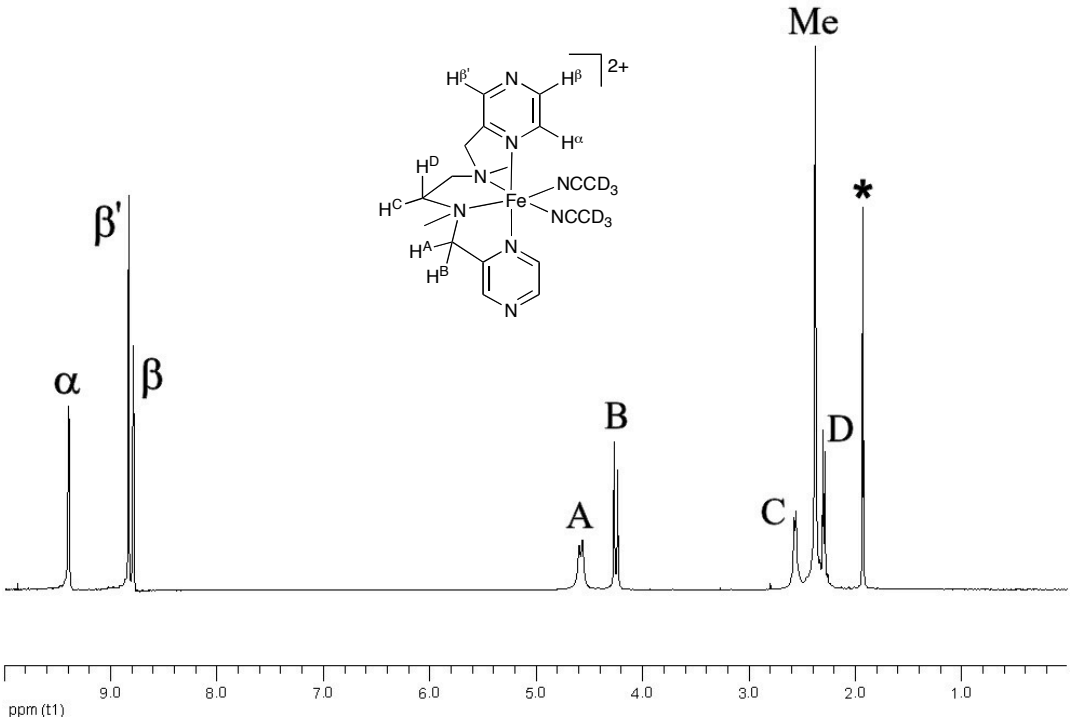

Figure 7. The ^{1}H-NMR spectrum of [Fe(**4**)$(CD_3CN)_2$]$(OTf)_2$, recorded in CD_3CN solution at 238 K (∗ = CH_3CN).

The ^{1}H-NMR spectrum of complex [Fe(**4**)(OTf)$_2$] in CD_2Cl_2 solution at room temperature is characteristic of a high-spin iron(II) complex (see Figure 8). In order to investigate whether complex [Fe(**4**)(OTf)$_2$] exhibits any spin-crossover behaviour or unusual fluxional behaviour in CD_2Cl_2 solution, VT ^{1}H-NMR spectra were measured over the liquid range of the solvent. A plot of the chemical shift of the individual resonances *versus* the reciprocal of temperature is given in Figure S7. The linear variation of the chemical shift is consistent with Curie law behaviour and the iron(II) centre being exclusively high-spin over the whole temperature range between 220-300K.

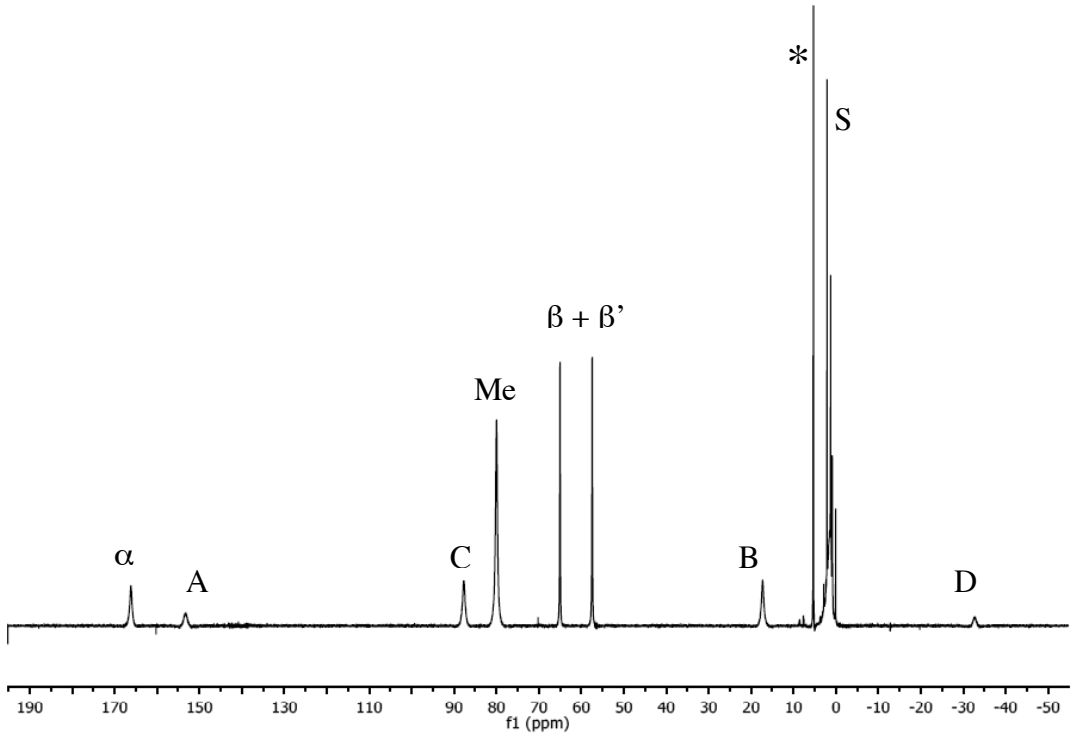

Figure 8. The ^{1}H NMR spectrum and corresponding peak assignment for [Fe(**4**)(OTf)$_2$], recorded in CD_2Cl_2 (∗) solution at 298 K. (**s**: solvent residues.)

The ^{1}H NMR spectra of the oxygen bridged complex [Fe(**5**)(OTf)$_2$] in CD_2Cl_2 and in CD_3CN are both paramagnetic at room temperature (Figures S8 and S9). This indicates that the bis(triflate) and the bis(acetonitrile) complexes (assumed to be formed in CD_3CN) are both high spin at room temperature, which is consistent with the magnetic moment measurements that show a high spin configuration in both solvents (*vide supra*). Similar observations were made for the phenylene bridged complex [Fe(**7**)(OTf)$_2$] (see Figure S12), for which a *trans* geometry was observed in

the solid state. On the basis of the similarities in the NMR and UV-vis spectra, the magnetic susceptibility and catalytic behaviour, we assign a *trans* configuration for both complexes [Fe(**5**)$(OTf)_2$] and [Fe(**7**)$(OTf)_2$].

Complexes [Fe(**6**)$(OTf)_2$] and [Fe(**8**)$(OTf)_2$] are paramagnetic in CD_2Cl_2, but in CD_3CN the VT ^{1}H NMR spectra show spin crossover behaviour (Figure S10 and S11). The softer sulphur donors in combination with two acetonitrile and two pyridine ligands create a strong ligand field, which leads to a LS configuration at low temperature, whereas at higher temperatures the HS configuration is observed. The ^{1}H NMR spectrum at these higher temperatures (e.g. 343K), shows only the pyridyl protons as sharp singlets, whereas the methylene protons are very broad, indicating considerable fluxional behaviour of the ligand backbone (see Figure S11). This indicates that these sulphur donors, despite their stronger coordination compared to the oxygen donors, do not enforce the same conformational rigidity as seen for the amine donors in the BPMEN complex [Fe(**1**)$(OTf)_2$].

The paramagnetic ^{1}H NMR spectra of [Fe(**10**)$(OTf)_2$], [Fe(**11**)$(OTf)_2$] and [Fe(**12**)$(OTf)_2$] in CD_2Cl_2 and CD_3CN solution can be assigned by comparison with the previously reported ^{1}H NMR spectra of complex [Fe(**9**)$(OTf)_2$].[24] The main difference between the spectra is the absence of the protons in the *para* position of the pyridine rings, which are typically observed at a chemical shift of 10-20 ppm. It was often observed for these complexes that insufficient numbers of resonances were found to account for all the methylene and ethylene protons or they were very broad due to fluxional behaviour, with the result that peak integration was unreliable. The exact number of methylene and ethylene resonances observed was found to depend on the solvent and the nature of the *para*-pyridyl substituent. Generally speaking, using CD_3CN as the NMR solvent led to observation of more of the ethylene and methylene proton resonances than with CD_2Cl_2.

^{19}F NMR Spectroscopy

The chemical shifts and half-height line widths of the CF_3 resonances observed in the ^{19}F NMR spectra of the iron(II) bis(triflate) complexes are listed in Table 3.

Table 3. ^{19}F NMR data for of iron(II) bis(triflate) complexes at 298K.

Complex	^{19}F CD_2Cl_2[a]		^{19}F CD_3CN[a]	
	δ (ppm)	$\nu_{1/2}$ (Hz)	δ (ppm)	$\nu_{1/2}$ (Hz)
[Fe(**1**)$(OTf)_2$] (BPMEN)	-29	716	-77	845
[Fe(**2**)$(OTf)_2$] (p-Cl)	-28	540	-79	740
[Fe(**3**)$(OTf)_2$] (p-OMe)	-24	1180	-74	1540
[Fe(**4**)$(OTf)_2$] (BPZMEN)	-33	820	-78	310
[Fe(**5**)$(OTf)_2$] (BPMEO)	-33	560	-60	400
[Fe(**6**)$(OTf)_2$] (BPMES)	-20	2400	-76	130
[Fe(**7**)$(OTf)_2$] (BPMPhO)	-35	750	-66	400
[Fe(**8**)$(OTf)_2$] (BPMPhS)	-21	2900	-77	450
[Fe(**9**)$(OTf)_2$] (*i*-BPMEN)	-24	1330	-66	920
[Fe(**10**)$(OTf)_2$] (p-Me)	-28	610	-69	410
[Fe(**11**)$(OTf)_2$] (p-Cl)	-26	1740	-64	1130
[Fe(**12**)$(OTf)_2$] (p-OMe)	-27	980	-72	280

The ^{19}F NMR data for all complexes in CD_2Cl_2 and CD_3CN solution are at first glance very similar. In CD_2Cl_2 solution, the triflate anions are coordinated to the iron centre, which results in a relatively broad peak between -20 and -30 ppm. The shift from ca. -80 ppm (for the free triflate anion) is caused by their proximity to the paramagnetic centre. There appears to be a correlation between the chemical shift values (δ) and the linewidths ($\nu_{1/2}$) observed in CD_2Cl_2 solution (see Figure S17). Complexes with stronger field ligands (for example **6** and **8** and perhaps also **3** and **9**) give rise to broader signals at lower chemical shift values, which is probably related to the rate of triflate exchange in these complexes. There is no apparent correlation in CD_3CN.

VT ^{19}F NMR measurements show a shift from ca. -30 ppm at 298 K to ca. -10 ppm at 188K for the complexes containing ligands **1** – **4** and from -20 ppm to ca. +10 ppm for those containing ligands **6** and **8**. For complex [Fe(**8**)$(OTf)_2$], a small amount of a triflate dissociated species is observed below 258K, most likely a five-coordinate complex [Fe(**8**)(OTf)]OTf (Figure S16). Triflate dissociation at lower temperature is also observed for complex [Fe(**5**)$(OTf)_2$], but in this case [Fe(**5**)(OTf)]OTf is the major species below 200K, whereas the *trans* complex [Fe(**7**)$(OTf)_2$] shows dissociation of both triflate anions at lower temperature (Figures S14 and S15). The reason for this anion dissociation at lower temperature is presumably due to the stabilisation of five- and four-coordinate complexes at lower temperatures.

In CD_3CN solution, the triflate anions exist mainly as non-coordinating counterions, which appear around -80 ppm. A minor peak (typically less than 5 %) around -20 ppm is also observed in the case of the complexes containing ligands **1**, **2** and **4**, indicating the presence of complexes with coordinated triflate ligands such as $[Fe(L)(CH_3CN)(OTf)]^+$, similar to previous observations made us and also by Comba and co-workers for $[Fe(bispidine)(OTf)_2]$ complexes in methanol solution.[26, 70] Rapid exchange between coordinated and uncoordinated triflate and acetonitrile ligands results in the observed signal broadening, consistent with $[Fe(L)(OTf)_2]$ being the dominant species in CD_2Cl_2 solution, whereas in CD_3CN solution, $[Fe(L)(CH_3CN)_2]^{2+}$ is the major complex and $[Fe(L)(CH_3CN)(OTf)]^+$ a minor species. The relatively strong field ligands **1**, **2** and **4** apparently slow down the exchange process to such a rate that the minor triflate-coordinated species becomes observable.

UV-Vis spectroscopy

The UV-Vis spectra of the iron(II) complexes $[Fe(L)(CH_3CN)_2]^{2+}$ where L = **1** – **12** generally feature high intensity bands in the UV region and broad transitions in the near-visible (Figures 9a-c, Table 4). Because several complexes in this study are in a spin crossover regime at room temperature, the electronic spectra are a combination of both the HS and LS component. By analogy to spectra of similar iron(II) complexes of pyridine-alkylamino ligands,[44, 70-73] the two sets of bands can be assigned to ligand-centred π-π* transitions and MLCT bands of the LS component, respectively. In those cases where a significant amount of the LS fraction is present, the weak $^1T_1 \leftarrow {}^1A_1$ transitions at approximately 500-550 nm can also be observed.[73]

Table 4. Selected physical parameters of iron(II) bis(triflate) complexes

Complex	MLCT		$^1T_1 \leftarrow {}^1A_1$		μ_{eff}[c] CD_3CN (μ_B)	T_c (K)
	λ (nm)	ε ($M^{-1}cm^{-1}$)	λ (nm)	ε ($M^{-1}cm^{-1}$)		
[Fe(**1**)$(OTf)_2$] (BPMEN)	375	3800	544	40	4.26	264
[Fe(**2**)$(OTf)_2$] (p-Cl)	383	3700	533	20	4.42	259
[Fe(**3**)$(OTf)_2$] (p-OMe)	340	1300			4.76	
[Fe(**4**)$(OTf)_2$] (BPZMEN)	432	6800			2.86	292
[Fe(**5**)$(OTf)_2$] (BPMEO)	334	540			4.96	
[Fe(**6**)$(OTf)_2$] (BPMES)	357	4800	558	90	2.82	287
[Fe(**7**)$(OTf)_2$] (BPMPhO)					5.17	
[Fe(**8**)$(OTf)_2$] (BPMPhS)	350	3800	533	95	2.64	287
[Fe(**9**)$(OTf)_2$] (*i*-BPMEN)	374	1100			4.72	238

[Fe(**10**)$(OTf)_2$] (p-Me)	368	960			4.79	
[Fe(**11**)$(OTf)_2$] (p-Cl)	386	1300			4.85	
[Fe(**12**)$(OTf)_2$] (p-OMe)	360	440			4.80	

a) c = 0.5 mM in CH_3CN. b) Evans' NMR method, 298 K.

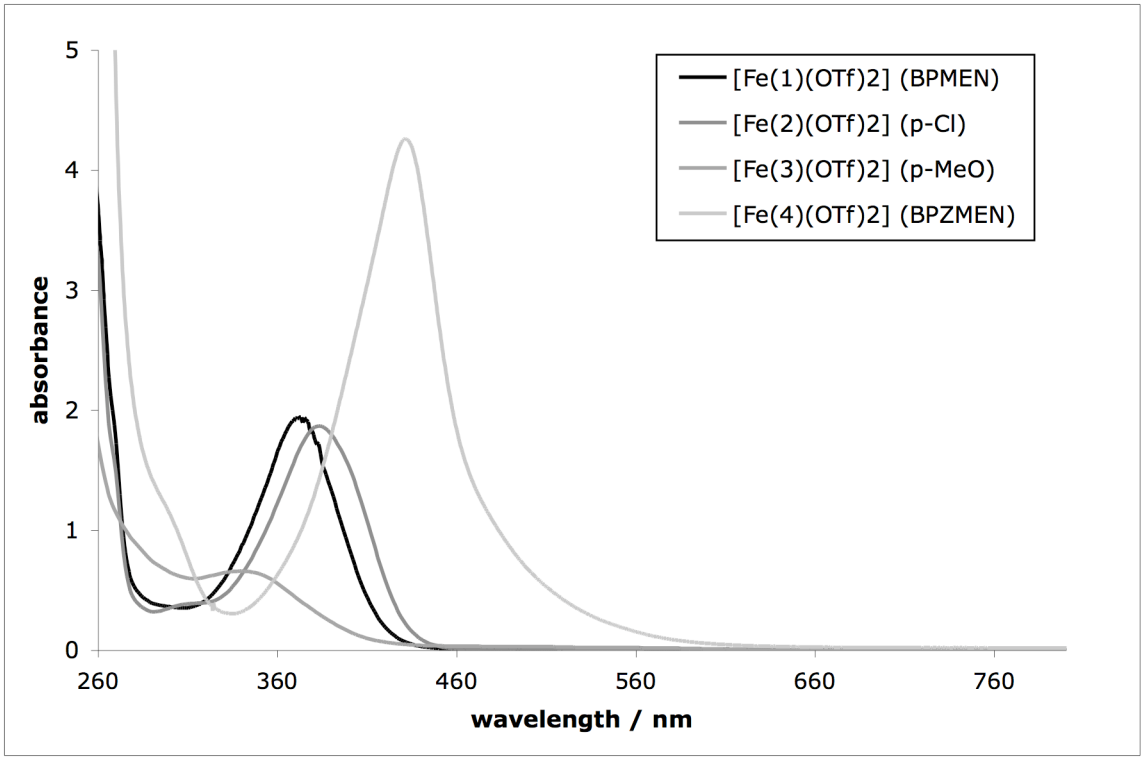

Figure 9a. The UV-vis spectra of $[Fe(L)(CH_3CN)_2]^{2+}$ complexes containing ligands **1**-**4** (0.5 mM, CH_3CN, 298K).

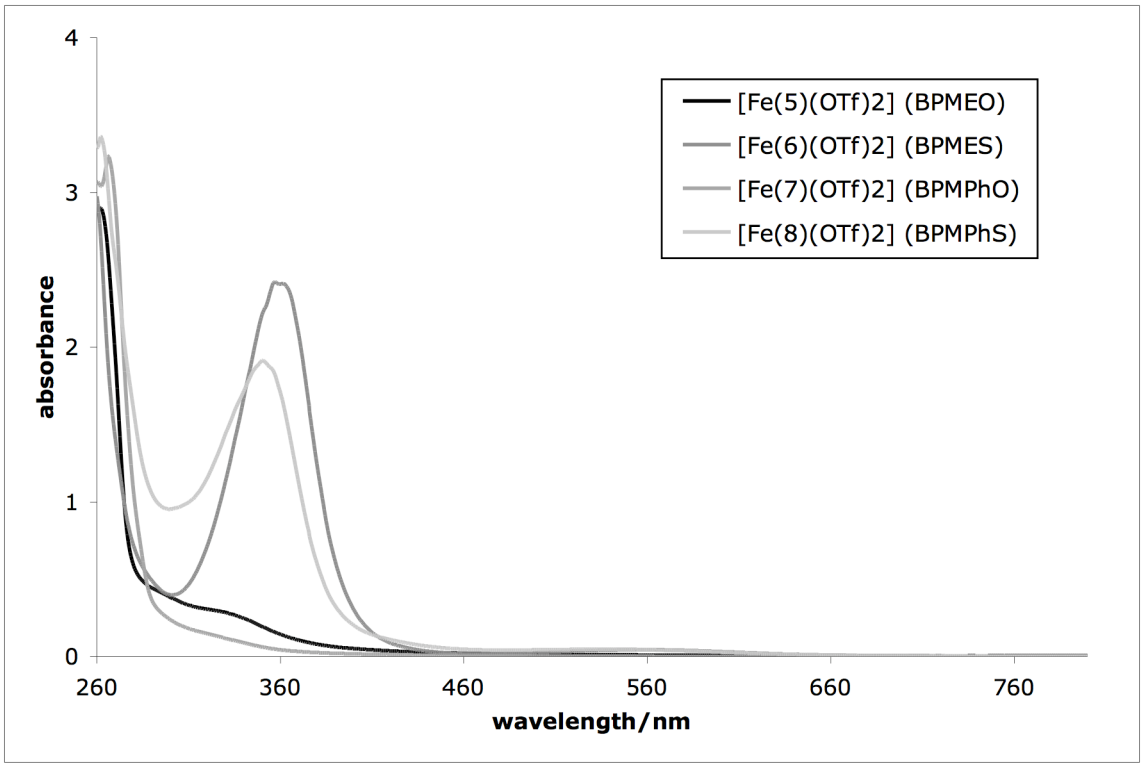

Figure 9b. UV-vis spectra of $[Fe(L)(CH_3CN)_2]^{2+}$ complexes containing ligands **5-8** (0.5 mM, CH_3CN, 298K).

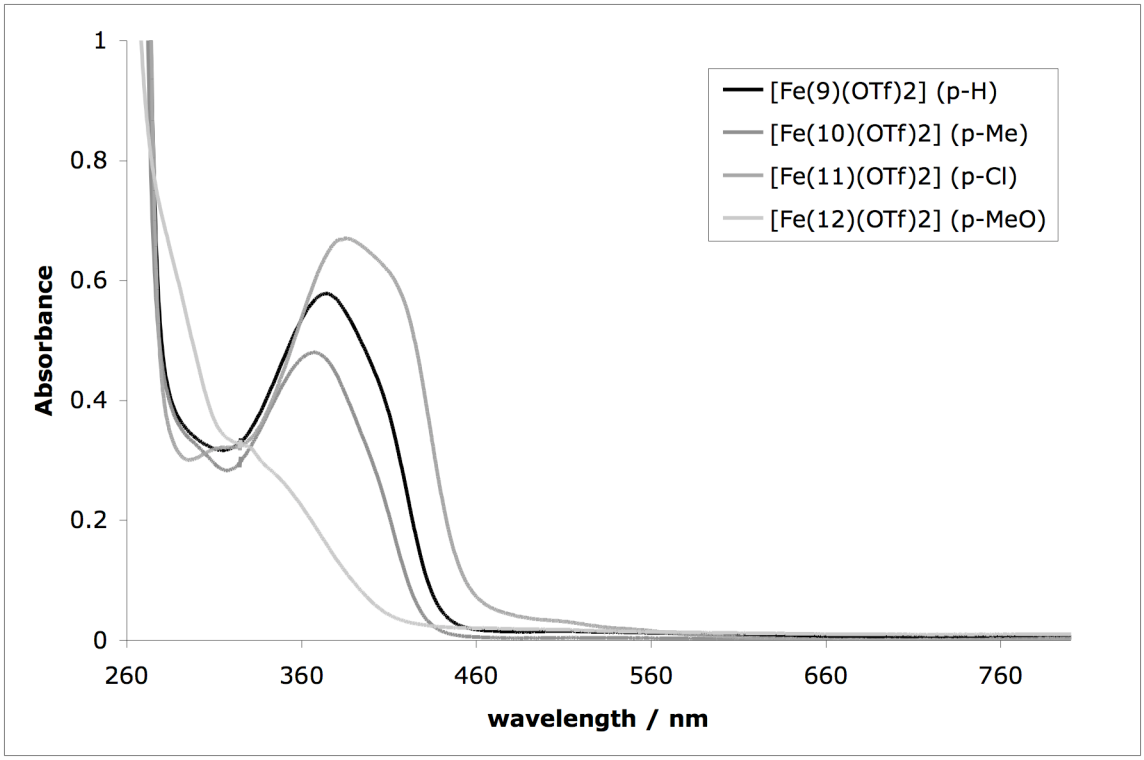

Figure 9c. UV-vis spectra of $[Fe(L)(CH_3CN)_2]^{2+}$ complexes containing iso-BPMEN ligands **9-12** (0.5 mM, CH_3CN, 298K).

The UV-vis spectra of complexes $[Fe(L)(CH_3CN)_2]^{2+}$ where L = **1**-**3** illustrate the effect of electron donating and withdrawing substituents in the *para* position of the pyridine ligands. The electron withdrawing chloro substituent results in a red shift of the MLCT band, whereas the electron-donating methoxy substituent induces the opposite effect. Comparable values for λ_{max} are obtained for the *iso*-bpmen ligand series of class III, where L = **9**-**12**, although the extinction coefficients are much smaller in this case. The *para*-methoxy substituent results in stronger sigma donation due to the increased basicity (pK_a = 6.58 for p-methoxypyridinium *versus* pK_a = 5.21 for pyridinium),[74] but back donation from metal to pyridine will be weaker, resulting in an overall weaker ligand field. Conversely, *para*-chloro pyridine is a weaker base and sigma donor (pK_a = 3.83 for *para*-chloro pyridinium), but increased back donation will result in a stronger ligand field. A weaker ligand field results in a decrease in the amount of LS complex and a decrease in the intensity of the MLCT absorption. Overall, these effects decrease λ_{max} and the intensity of the MLCT absorption in the order Cl > H > Me > OMe, as can be seen in the BPMEN series (see Figure 9a, although the *para*-chloro substituent has only a small effect on ε_{max} in this case) and more clearly in the *iso*-BPMEN series shown in Figure 9c.

One of the most salient features of the UV-vis spectra in Figure 9a is the large extinction coefficient of the MLCT band of complex $[Fe(\mathbf{4})(CH_3CN)_2]^{2+}$ at 432 nm (ε_{max} = 6800 $M^{-1}cm^{-1}$), which is much larger than any of the other complexes. Pyrazine has lower lying π* orbitals and is therefore a better π-acceptor ligand than pyridine.[69, 75] It is also a much weaker base (pK_a = 0.65 for pyrazinium *versus* pK_a = 5.21 for pyridinium) and consequently a much poorer σ-donor. This will lower the energy of the metal d-orbitals significantly, consistent with the observed increase in the oxidation potential from E_{ox} = 1.15 V for $[Fe(\mathbf{1})(CH_3CN)_2]^{2+}$ compared to E_{ox} = 1.37 V for $[Fe(\mathbf{4})(CH_3CN)_2]^{2+}$ and a shift of the MLCT band from 375 nm to 432 nm. The differences in extinction coefficient are most likely due to the increased fraction of LS *versus* HS complex at 298K for $[Fe(\mathbf{4})(CH_3CN)_2]^{2+}$, as shown by the magnetic susceptibility measurements in acetonitrile solution (see next section).

The UV-vis spectra for the second class of complexes containing oxygen and sulfur atoms as the central donors are shown in Figure 9b. The sulfur donors result in spin crossover systems $[Fe(\mathbf{6})(CH_3CN)_2]^{2+}$ and $[Fe(\mathbf{8})(CH_3CN)_2]^{2+}$, with significant

amounts of the LS fraction generating a strong MLCT absorption around 350-360 nm. The oxygen donors are only weak field ligands, resulting in a weak MLCT absorption in the case of $[Fe(\mathbf{5})(CH_3CN)_2]^{2+}$, whereas no MLCT absorption can be detected for complex $[Fe(\mathbf{7})(CH_3CN)_2]^{2+}$ which, as seen in the solid state structure, contains a *trans* coordination geometry.

Magnetic Susceptibilities

Magnetic susceptibility measurements have been used in this study to measure the relative ligand field strength of the different ligands **1** – **12** in octahedral iron(II) complexes. In CD_2Cl_2 solution, the bis(triflate) complexes display magnetic moments of $\mu_{eff} \approx 5$ BM, consistent with HS iron(II) ($S = 2$) centres, due to the weak ligand field exerted by triflate anions. In CD_3CN solution, the triflate anions are displaced by stronger field acetonitrile ligands to yield dicationic complexes of the form $[Fe(L)(CH_3CN)_2]^{2+}$. The magnetic moments of the iron(II) bis(triflate) complexes, measured in CD_3CN solution at 298 K using the Evans' NMR method, are listed in Table 4, including the previously reported data for $[Fe(\mathbf{1})(OTf)_2]$ and $[Fe(\mathbf{9})(OTf)_2]$ for comparison.[24] For several complexes, the μ_{eff} values are significantly lower than expected for a HS iron(II) centre, which is suggestive of the existence of spin crossover (SC) behaviour in these complexes.[68, 76-78]

The magnetic behaviour of the iron(II) complexes in CD_3CN solution was investigated in more detail by measurement of their magnetic moments over the temperature range 233-343 K using the Evans' NMR method (Figure 10). The complexes with the strongest ligand field which are those containing ligands **1**, **2**, **4**, **6** and **8** undergo nearly a full spin transition within the temperature range (233-343K). For these complexes, the critical temperatures T_c (the temperature where the amounts of high spin and low spin are equal) are listed in Table 4. The two iron(II) complexes containing the oxygen bridged ligands **5** and **7** induce the weakest ligand field and remain high spin down to 233K. The complexes of the *iso*-BPMEN series (ligands **9**-**12**) and the *para*-methoxy substituted BPMEN complex $[Fe(\mathbf{3})(CH_3CN)_n]^{2+}$ show a decrease of the magnetic moment at lower temperatures, indicative of a partial spin transition within the temperature range and have therefore an intermediate ligand field

strength. The strongest ligand field is observed for the pyrazyl complex $[Fe(\mathbf{4})(CH_3CN)_n]^{2+}$, which has the highest critical temperature T_c of 292 K.

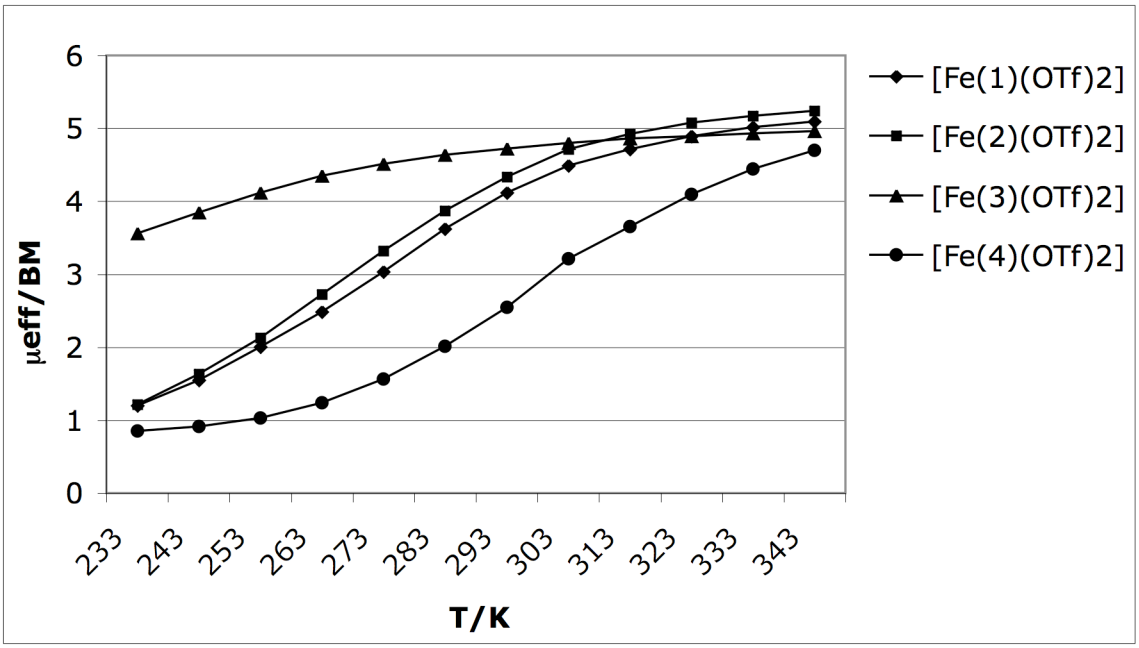

Figure 10a. The magnetic moments of iron(II) complexes containing ligands **1** – **4** in CD_3CN solution as a function of temperature.

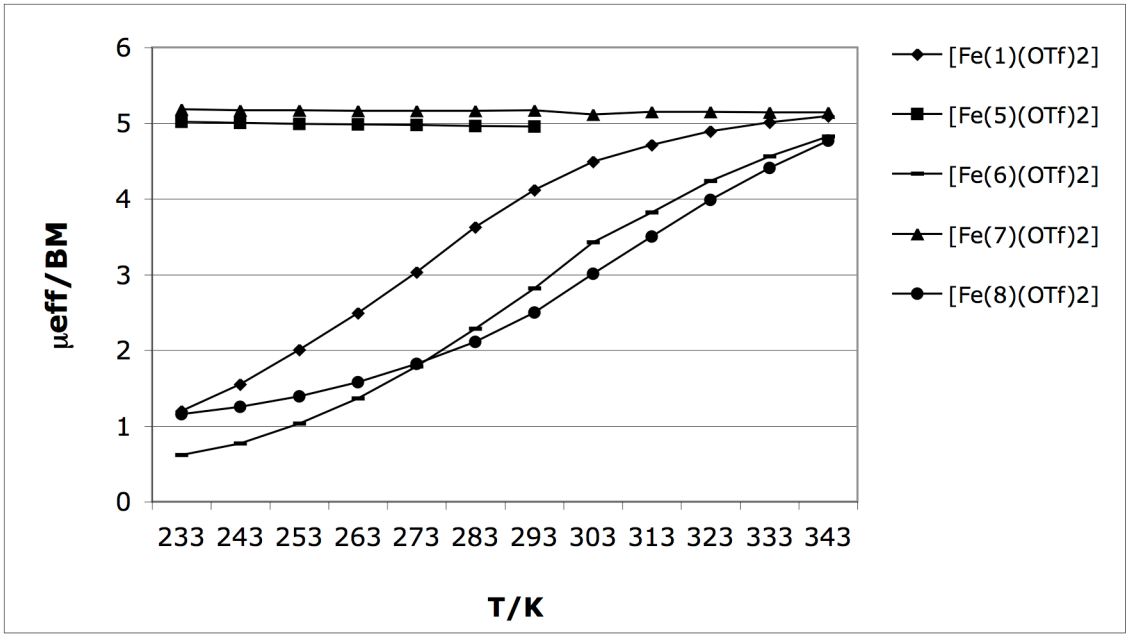

Figure 10b. The magnetic moments of iron(II) complexes containing ligands **5** – **8**, together with complex $[Fe(\mathbf{1})(OTf)_2]$ for comparison, in CD_3CN solution as a function of temperature.

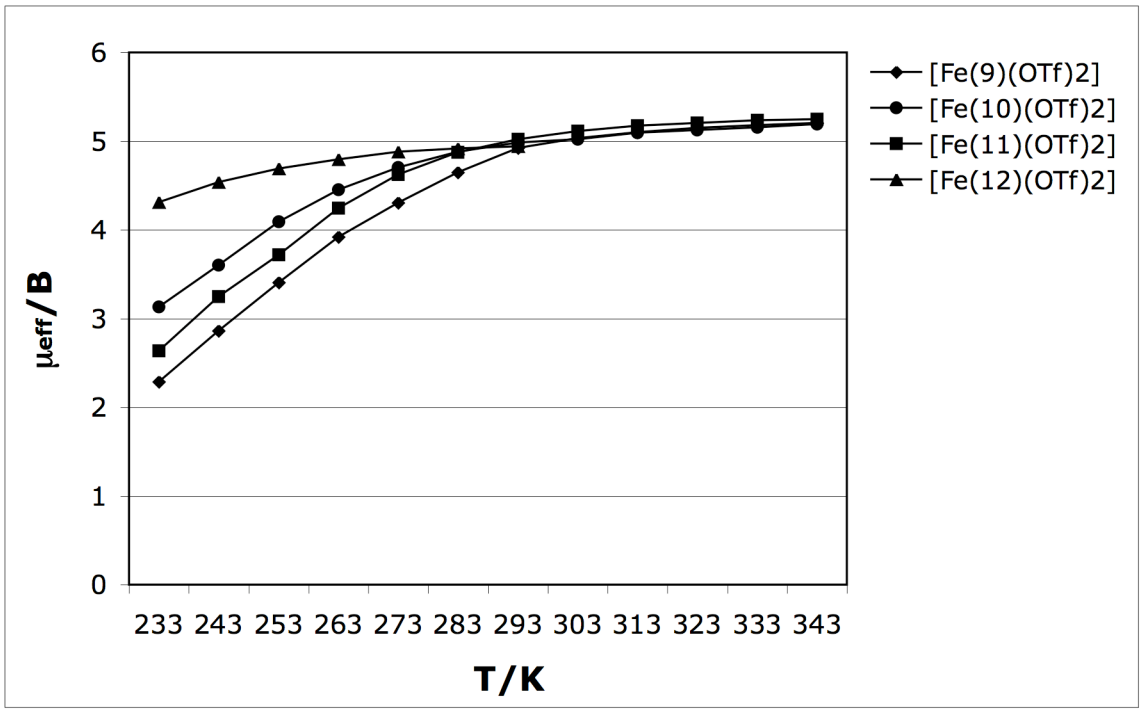

Figure 10c. The magnetic moments of iron(II) complexes containing ligands **9** – **12** in CD_3CN solution as a function of temperature.

Catalytic Oxidation of Alkanes

The catalytic properties of the iron(II) bis(triflate) complexes containing ligands **1** – **12** for the oxidation of cyclohexane with H_2O_2 have been evaluated (Eq. 1).

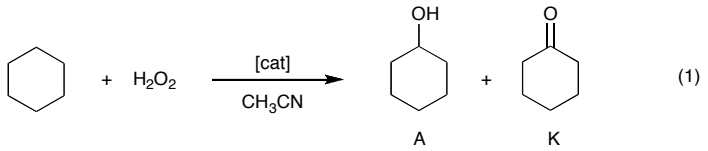

The oxidation reactions were carried out under our standard conditions in order to compare the results with previously reported data (see Supporting Information).[26, 44] Hydrogen peroxide solution (10 equiv. or 100 equiv.) was added to an acetonitrile solution containing the catalyst (1 equiv.) and cyclohexane (1000 equiv). A large excess of substrate was used to minimize over-oxidation of cyclohexanol (A) to cyclohexanone (K). The addition of dilute H_2O_2 was carried out slowly using a syringe pump, in order to minimise H_2O_2 decomposition. The yields are based on the amount of oxidant (H_2O_2) converted into oxygenated products. All the individual catalytic runs were performed at least twice.

Two series of catalytic experiments were carried out initially, using 10 and 100 equiv. of H_2O_2. The amount of cyclohexanol (A) and cyclohexanone (K) are measured by GC and the percentage conversion of H_2O_2 into oxidised products (A + K) for the different catalysts is shown in Table 5. The iron bis(triflate) complex [Fe(**1**)$(OTf)_2$], containing the ligand BPMEN, is used as a benchmark against which the other catalysts are compared. We have previously reported that this catalyst, when using 10 equiv. of H_2O_2, converts 65% of the added H_2O_2 into oxygenated products, with a large ratio of cyclohexanol to cyclohexanone (A/K ratio) of 9.[43] These results are consistent with those reported previously by Que and co-workers for the complex [Fe(**1**)$(CH_3CN)_2$]$(ClO_4)_2$.[30] The results obtained with [Fe$(OTf)_2(CH_3CN)_2$] have been added for comparison (runs 17 and 18), which show only low conversions and A/K ratios, indicative of Fenton-type behaviour.

Table 5. Oxidation of cyclohexane with H_2O_2 catalysed by [Fe(L)$(OTf)_2$].[a]

Run	catalyst	Equiv. H_2O_2	A + K [b] (%)	A/K [c]
1[d]	[Fe(**1**)$(OTf)_2$] (BPMEN)	10	65	9.5
2[d]	[Fe(**1**)$(OTf)_2$] (BPMEN)	100	48	2.5
3	[Fe(**2**)$(OTf)_2$] (p-Cl)	10	53	7.1
4	[Fe(**2**)$(OTf)_2$] (p-Cl)	100	41	2.7
5	[Fe(**3**)$(OTf)_2$] (p-OMe)	10	53	11.0
6	[Fe(**3**)$(OTf)_2$] (p-OMe)	100	45	3.6
7	[Fe(**4**)$(OTf)_2$] (BPZMEN)	10	38	2.3
8	[Fe(**4**)$(OTf)_2$] (BPZMEN)	100	20	1.7
9[e]	[Fe(**9**)$(OTf)_2$] (*i*-BPMEN)	10	32	6.8
10[e]	[Fe(**9**)$(OTf)_2$] (*i*-BPMEN)	100	6.6	4.4
11	[Fe(**10**)$(OTf)_2$] (p-Me)	10	34	6.6
12	[Fe(**10**)$(OTf)_2$] (p-Me)	100	6.1	5.3
13	[Fe(**11**)$(OTf)_2$] (p-Cl)	10	16	3.3
14	[Fe(**11**)$(OTf)_2$] (p-Cl)	100	4.4	4.0
15	[Fe(**12**)$(OTf)_2$] (p-OMe)	10	28	4.7
16	[Fe(**12**)$(OTf)_2$] (p-OMe)	100	4.1	4.7
17	[Fe$(OTf)_2(CH_3CN)_2$]	10	3.8	1.6

18	$[Fe(OTf)_2(CH_3CN)_2]$	100	3.4	2.4

[a] Catalytic conditions: see Experimental section. [b] Total percentage yield of cyclohexanol (A) + cyclohexanone (K), expressed as moles of product per mole of H_2O_2. [c] Ratio of moles of cyclohexanol (A) to moles of cyclohexanone (K). [d] Data taken from Ref. 44. [e] Data taken from Ref. 24.

The results in Table 5 show clear differences between the various classes of iron(II) catalysts. The first set of catalysts containing ligands **1** – **4** (runs 1-8) shows conversions of ca. 40-65 % H_2O_2 into oxidised products, using 10 equiv. of H_2O_2. Increasing the amount of H_2O_2 to 100 equivalents leads to more oxidised product, but this lowers the percentage conversion of H_2O_2 (20-50%). The second class of catalysts containing ligands **5** – **8** with sulphur and oxygen donors showed no oxidation activity at 10 or 100 equiv. of H_2O_2 added. The ligands with the oxygen donors (**5** and **7**) have been shown by the NMR and magnetic moment measurements to create only weak ligand fields and the iron(II) complexes are high spin in acetonitrile solution. Ligand displacement and catalyst decomposition are likely in this case. The sulphur bridged ligands **6** and **8** generate a much stronger ligand field, but the sulphur donors are prone to oxidation to form sulphoxides. The third class containing the *iso*-BPMEN ligand series **9** - **12** gave reasonable conversions of 15-30 % at the lower oxidant loading, but this percentage decreased to 4-7 % at 100 equiv. H_2O_2. These catalysts are generally less active than the catalysts in the first class and appear to deactivate more rapidly. In order to discern any electronic effects caused by the *para* substituents of the pyridine donors, the performance of the catalysts of class I was investigated in more detail by monitoring the amount of oxidised product produced with various amounts of H_2O_2 (Figure 11).

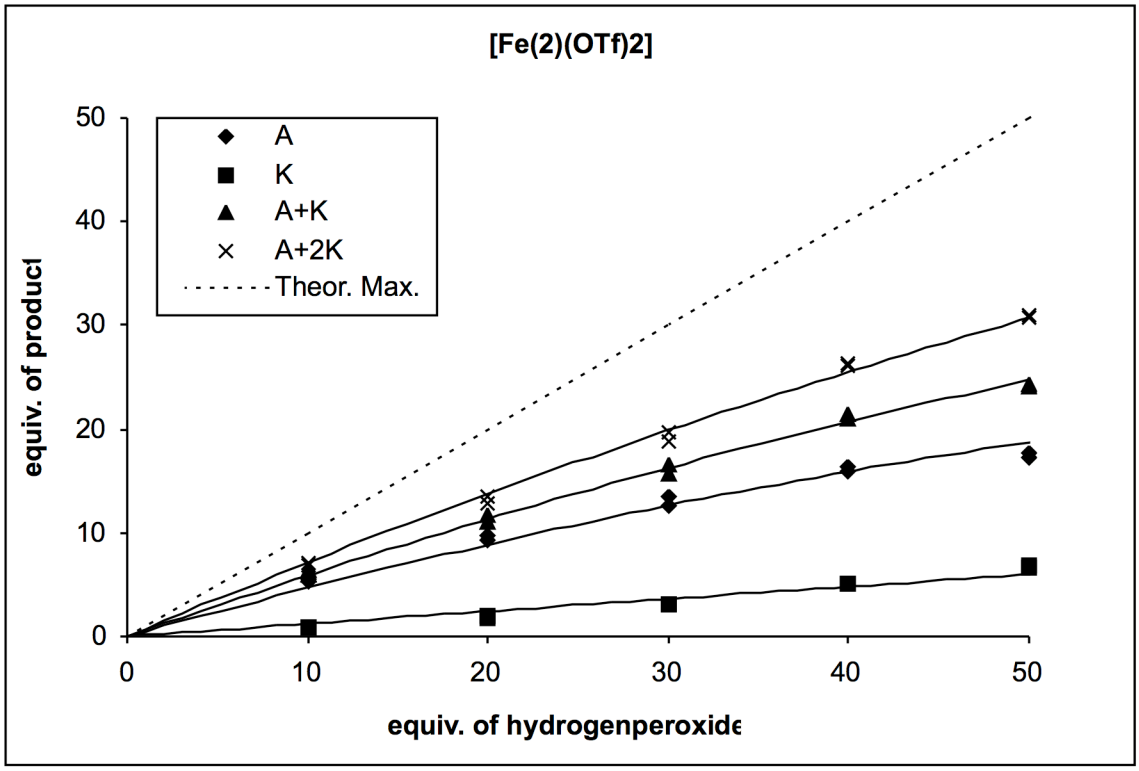
[Fe(2)(OTf)2]
A
K
A+K
A+2K
Theor. Max.
equiv. of product
equiv. of hydrogenperoxide
0
10
20
30
40
50

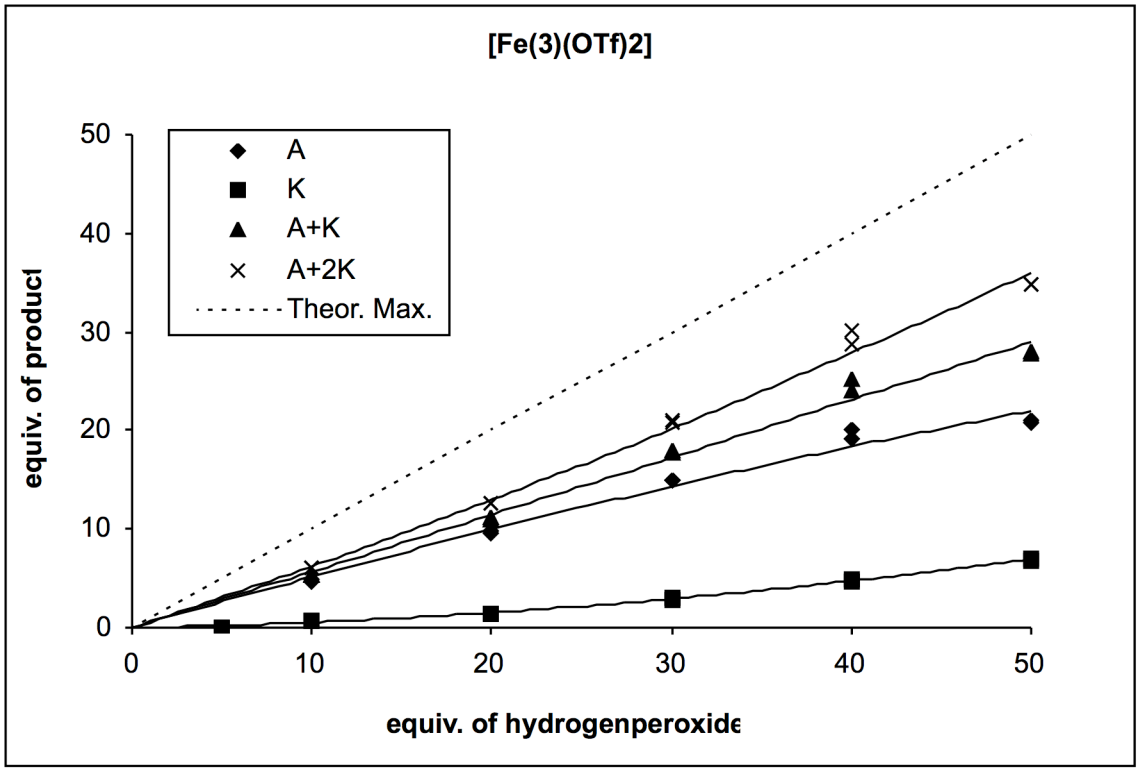
[Fe(3)(OTf)2]
A
K
A+K
A+2K
Theor. Max.
equiv. of product
equiv. of hydrogenperoxide
0
10
20
30
40
50

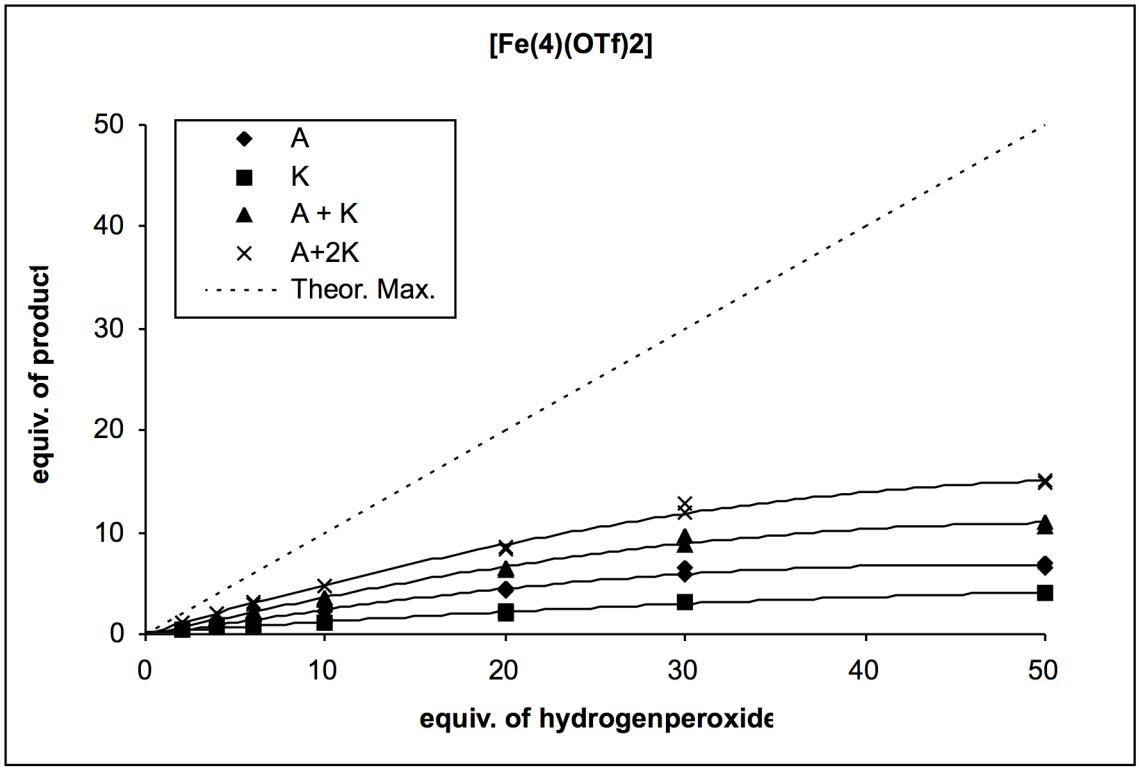

Figure 11. Product composition at various amounts of H_2O_2 in the oxidation of cyclohexane catalyzed by [Fe(**2**)$(OTf)_2$] (top), [Fe(**3**)$(OTf)_2$] (middle) and [Fe(**4**)$(OTf)_2$] (bottom). The dashed line represents the total number of equivalents of oxidised product that can be obtained.

The dashed diagonal line is included in Figure 11 to represent the total number of equivalents of oxidised product that can be obtained from any amount of H_2O_2 added. It appears that the addition of more H_2O_2 leads to more cyclohexanol (A) and cyclohexanone (K), but the relationship is not linear. If we consider that a second equivalent of oxidant is required to oxidise cyclohexanol to cyclohexanone, the total conversion of H_2O_2 to generate the oxygenated products is given by the sum of the equivalents of cyclohexanol and twice the equivalents of cyclohexanone produced, which is represented by the A+2K curves in Figure 11.

In order to compare the efficiency of the most active catalysts, their A+2K curves have been collected in Figure 12. The previously reported measurements for complexes [Fe(**1**)$(OTf)_2$] and [Fe(**9**)$(OTf)_2$] are included for comparison. It can be seen that the A+2K curves for complexes [Fe(**1**)$(OTf)_2$], [Fe(**2**)$(OTf)_2$] and [Fe(**3**)$(OTf)_2$] are very similar. The methoxy-substituted complex [Fe(**3**)$(OTf)_2$]

appears to give a slightly better performance, especially at higher H_2O_2 loadings (see also Table 5, runs 5 and 6). This could be related to the increased basicity of the *para*-methoxy pyridine donor, resulting in an increased stability of this catalyst. The activity of complex [Fe(**4**)(OTf)$_2$] containing the pyrazine donors decreases more rapidly, which indicates faster catalyst degradation in this case, probably related to the weaker binding of pyrazine *versus* pyridine. The A + 2K curve for complex [Fe(**9**)(OTf)$_2$] has also been included and it can be seen that this complex and also the other complexes containing the *para*-substituted ligands **10**, **11** and **12** suffer from rapid deactivation. No apparent effect due the para substituent on the catalytic activity could be observed for these complexes.

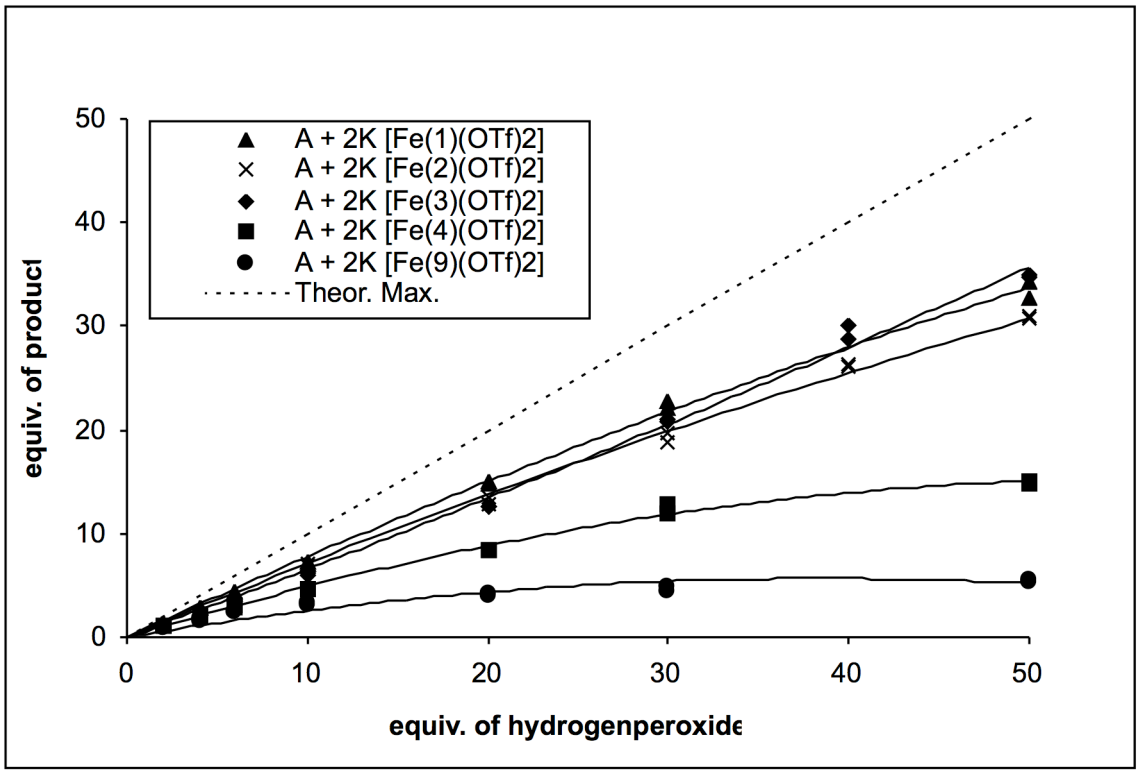

Figure 12. Conversion of H_2O_2 into oxygenated products (A+2K curves) for different catalysts. The dashed line represents the total number of equivalents of oxidised product that can be obtained.

In conclusion, the UV-vis spectroscopy studies and the magnetic susceptibility measurements have shown that electron donating or withdrawing substituents in the *para* position of the pyridine donors in BPMEN-type complexes of class I and *iso*-BPMEN type complexes of class III affect the electronic and magnetic properties of

these complexes. Electron donating substituents increase the basicity and the σ-donating ability of the pyridine ligand, but decrease the back bonding, resulting in an overall weakening of the ligand field, whereas electron-withdrawing substituents have the opposite effect. However, within a given class, the catalytic behaviour of the catalysts for the oxidation of cyclohexane by H_2O_2 is largely unaffected by the nature of the *para* substituents. These results consolidate our earlier hypothesis that the catalytic activity of non-heme iron complexes (and possibly also heme-type complexes) is largely controlled by the stability of the catalysts under the oxidising conditions. The methoxy-substituted catalyst [Fe(**3**)$(OTf)_2$] contains the most basic pyridine donors and this catalyst appears to give a slightly better performance. The degradation of these catalysts occurs probably by oxidation of the aliphatic C-H bonds of the ligand, possibly followed by further rearrangement of the ligand, eventually leading to de-complexation of the ligand from the metal centre. Other oxidisable moieties, such as sulphur donors are also likely to be oxidised and this will weaken their coordinating properties. In addition, any deviation from the *cis*-α coordination geometry to *cis*-β or *trans* geometries in these complexes results in a weaker ligand field and less active catalysts. We are currently investigating the deactivation processes in these non-heme iron catalysts, with the aim to increase their activity and lifetime so that they will become robust and practical catalysts for alkane oxidation reactions.

Experimental

General

All moisture and oxygen sensitive compounds were prepared using standard high vacuum line, Schlenk and cannula techniques. A standard nitrogen-filled glove box was used for any subsequent manipulation and storage of these compounds. Standard ^1H, ^{19}F and ^{13}C NMR spectra were recorded using a Bruker AC-250 MHz spectrometer. VT-NMR and COSY spectra were recorded using a Bruker AM-500 MHz or a DRX-400 MHz spectrometer. ^1H NMR were referenced to the residual non-deuterated solvent signal and ^{13}C NMR chemical shifts to the signal of the deuterated solvent. The ^{19}F NMR chemical shifts were referenced to $CFCl_3$. Mass spectra were recorded using either a VG Autospec or a VG Platform II spectrometer. Elemental analyses were performed by the Science Technical Support Unit at The

London Metropolitan University. GC analysis was performed using an Agilent 6890A gas chromatograph on either a HP-5 (30 m × 0.32 mm, film thickness 0.25 mm) or an Innowax (30 m × 0.25 mm, film thickness 0.25 mm) column. Toluene was used as the standard for quantitative analysis and product identities were confirmed using GC-MS. UV-vis spectra were recorded at 298K in acetonitrile solution using a Perkin-Elmer Lambda 20 spectrometer. Detailed experimental procedures for VT-Evans magnetic susceptibility measurements, as well as the standard testing conditions for the oxidation of cyclohexane can be found in the Supplementary Information.

Solvents and Reagents

Diethyl ether and tetrahydrofuran were dried by prolonged reflux, under a nitrogen atmosphere, over sodium metal with a benzephenone ketyl indicator and distilled freshly prior to use. Dichloromethane and acetonitrile were treated in a similar manner, but using calcium hydride as the drying agent. Toluene and pentane were dried by passing through a column, packed with commercially available Q-5 reagent (13 % CuO on alumina) and activated alumina (pellets, 3 mm), in a stream of nitrogen. The synthesis of the complexes $[Fe(OTf)_2(CH_3CN)_2]$,[79] $[Fe(\mathbf{1})(OTf)_2]$ and $[Fe(\mathbf{9})(OTf)_2]$[24] have been reported previously. The ligand precursors and ligands, N,N'-bis(2-pyrazylmethyl)ethylene-1,2-diamine,[55] N,N'-dimethyl-N,N'-bis(4-chloropyridylmethyl)ethylene-1,2-diamine (**2**),[53] N,N'-dimethyl-N,N'-bis(4-methoxypyridylmethyl)ethylene-1,2-diamine (**3**),[54] and S,S'-bis(2-pyridylmethyl)-1,2-ethanedithiol (BPMES) (**6**),[57] were all prepared according to published procedures.

Synthesis of the ligands

N,N'-bis(2-pyrazylmethyl)-N,N'-dimethylethyl-1,2-diamine (BPZMEN) (4): A mixture of N,N'-bis(2-pyrazylmethyl)ethylene-1,2-diamine, (0.55 g, 2.25 mmol), acetic acid (8.25 mL), 35 % w/w aqueous formaldehyde (3.00 mL, 35.1 mmol) and acetonitrile (45 mL) was stirred for 1 hour. Subsequent to this period, 0.57 g (15.1 mmol) of sodium borohydride was slowly added and the resultant mixture allowed to stir for a further 2 days. All volatiles were removed and the residue made strongly basic (pH ≥ 12). The aqueous layer was extracted with DCM (3×100 mL), the organic fractions combined, dried ($MgSO_4$) and all volatiles removed to give the product as a

yellow oil (0.47 g, 77 %). ^{1}H-NMR ($CDCl_3$): δ 8.65 (d, 2H, *J*=1Hz, 6-Pz*H*), 8.48 (dd, 2H, *J*=1 and 2.6Hz, 5-Pz*H*), 8.41 (d, 2H, *J*=2.6Hz, 3-Pz*H*), 3.71 (s, 4H, PzCH_2), 2.63 (s, 4H, NCH_2CH_2N), 2.27 (s, 6H, N*Me*). ^{13}C-NMR ($CDCl_3$): δ 154.8 (*ipso*), 145.2, 143.8, 143.1, 61.8 (Pz*C*H_2), 55.5 (N*C*H_2*C*H_2), 42.8 (N*Me*). MS (EI): *m/z* (%) 272 (4) [M^+], 179 (6) [(M-PzCH_2)$^+$], 149 (6) [(M-PzCH_2NHMe)$^+$], 136 (100) [(PzCH_2NMeCH_2)$^+$], 93 (34) [(PzCH_2)$^+$].

O,O'-bis(2-pyridylmethyl)-1,2-ethanediol (BPMEO) (5): NaH (0.44 g, 18.3 mmol) was dissolved in dry DMSO for 15 minutes, after which dry ethylene glycol (0.57 g, 9.15 mmol) was added dropwise and the solution was left to stir at room temperature for one hour. 2-Chloromethyl pyridine (2.54 g, 19.9 mmol, prepared from 2-chloromethyl pyridine hydrochloride and ammonia in chloroform) was added, dissolved in DMSO, to the reaction mixture, which subsequently turned red. The solution was left to stir for 15 hours at room temperature. The resulting dark brown solution was first dissolved in DCM, then water was added and the product was extracted three times with DCM, washed with water and the combined organic fractions were dried over sodium sulphate. The crude product was purified with by column chromatography using DCM:MeOH (98:2) to obtain a clear light brown oil. (0.56 g, 24%). ^{1}H NMR ($CDCl_3$): 8.54 (d, 2H, *J*=4Hz, pyrH), 7.68 (t, 2H, *J*=8Hz, pyrH), 7.49 (d, 2H, *J*=8Hz, pyrH), 7.18 (dd, 2H, *J*=4 and 8Hz, pyrH), 4.72 (s, 4H, pyrCH_2), 3.81 (s, 4H, OCH_2). ^{13}C NMR ($CDCl_3$): 158.47, 149.00, 136.65, 122.33, 121.35, 74.09 (pyr*C*H_2), 70.23 (O*C*H_2). MS (EI): *m/z* (%) 152 (35) [(PyCH_2O(CH_2)$_2$O)$^+$], 108 (38) [(PyCH_2O)$^+$], 92 (100) [PyCH_2^+].

O,O'-bis(2-pyridylmethyl)-1,2-phenylenediol (BPMPhO) (7): A mixture of 1,2-dihydroxybenzene (2.08 g, 18.89 mmol), 2-chloromethylpyridine hydrochloride (6.197 g, 37.78 mmol) and tetra(n-butyl)ammonium bromide was refluxed in benzene (50 ml) and 40% aqueous sodium hydroxide (8 ml) for 24h. The solution was left to cool down and then water was added. The organic layer was extracted with benzene, washed with water, dried with Na_2SO_4 and concentrated to give the crude product, which was purified by column chromatography using ethylacetate/n-hexane (3:1) to

give a pure beige crystalline product (0.85 g, 15%). ^{1}H NMR ($CDCl_3$): 8.6 (d, 2H, *J*=4Hz, pyrHα), 7.70 (t, 2H, *J*=8Hz, pyrH), 7.62 (d, 2H, *J*=8Hz, pyrH), 7.22 (dd, 2H, *J*=4.0Hz, *J*=8.0Hz, pyrH), 6.96 (m, 2H, ArH), 6.9 (m, 2H, ArH), 5.33 (s, 4H, C*H*$_2$). ^{13}C NMR ($CDCl_3$): 157.58, 149.12, 148.41, 136.84, 122.56, 121.74, 121.22, 114.48, 71.68 (*C*H_2). MS (EI): *m/z* (%) 292 (10) [M^+], 200 (71) [$(C_{12}H_{10}O_2N_2)^+$], 92 (100) [pyr-CH_2^+].

S,S'-bis(2-pyridylmethyl)-1,2-phenylenedithiol (BPMPhS) (8): Sodium (0.18 g, 7.03 mmol) was dissolved in ethanol (25 mL). To this solution benzene-1,2-dithiol (0.5 g, 3.52 mmol) was added followed by a solution of 2-(chloromethyl)pyridine (7.03 mmol) in ethanol (10 mL). The solution was heated to the point of reflux for 20 hours. Once cooled down water (50 mL) was added which dissolved the precipitate. The resulting solution was extracted with DCM (3 x 50 mL). The combined organic phase was washed with water (3 x 50 mL) and dried over Na_2SO_4. All solvents were removed to yield an orange oil (0.92 g, 81%). ^{1}H NMR ($CDCl_3$): δ 8.55 (d, 2H, *J*=1.8 Hz, 6-Py*H*), 7.62 (td, 2H, *J* =7.8 and 1.8 Hz, 4-Py*H*), 7.32 (d, 2H, *J*=7.8 Hz, 3-Py*H*), 7.26 (m, 2H, 3,6-Ph*H*), 7.18 (m, 2H, 5-Py*H*), 7.07 (m, 2H, 4,5-Ph*H*), 4.30 (s, 4H, PyC*H*$_2$). ^{13}C NMR ($CDCl_3$): δ 157.3, 149.0, 137.0, 137.5, 130.1, 127.0, 123.3, 122.2, 39.6. MS (+EI): *m/z* (%) 324 (24)[M^+], 232 (42) [$(M - PyCH_2)^+$], 231 (46), 200 (49) [$(M - PyCH_2S)^+$], 153 (65), 93 (100) [$(PyCH_3)^+$].

N,N-bis[2-(4-picolyl)methyl]-N',N'-dimethylethyl-1,2-diamine (Me-iso-BPMEN) (10): A mixture of N,N-dimethylethylene-1,2-diamine (0.41 mL, 3.68 mmol) and 4-methylpyridine-2-carboxaldehyde (1.16 g, 9.58 mmol) was stirred in DCM (50 mL) for 1 hour. Subsequently, this solution was to added to a suspension of sodium tri(acetoxy)borohydride in DCM (50 mL) and stirred for 18 hours. The reaction mixture was quenched by the addition of saturated aqueous sodium hydrogen carbonate solution. The organic layer was separated and the aqueous layer extracted with DCM (2×100 mL). All organic fractions were combined, dried ($MgSO_4$) and the solvent removed using a rotary evaporator. The impure yellow oil obtained was then dissolved in THF and added to a stirring suspension of KH (0.074 g, 1.84 mmol) in THF. After stirring for 90 minutes, all volatiles were removed *in vacuo* and the residue extracted with pentane (3×100 mL). The pentane extracts were combined,

filtered and reduced to dryness to give **10** as a viscous yellow oil (0.65g, 59 %). ^{1}H-NMR ($CDCl_3$): δ 8.29 (d, 2H, *J*=5Hz, 6-Py*H*), 7.25 (s, 2H, 3-Py*H*), 6.88 (d, 2H, *J*=5Hz, 5-Py*H*), 3.75 (s, 4H, PyC*H*$_2$), 2.61 (m, 2H, PyCH$_2$NC*H*$_2$), 2.42 (m, 2H, C*H*$_2$NMe$_2$), 2.26 (s, 6H, Py*Me*), 2.10 (s, 6H, N*Me*). ^{13}C-NMR ($CDCl_3$): δ 159.1 (*ipso*), 148.5, 147.2 (*ipso*), 123.8, 122.8, 60.6 (Py*CH*$_2$), 57.1 (N*CH*$_2$), 52.0 (N*CH*$_2$), 45.5 (N*Me*), 20.9 (Py*Me*). MS (EI): *m*/*z* (%) 298 (4) [M^+], 253 (1) [$(M\text{-}HNMe_2)^+$], 240 (100) [$(M\text{-}Me_2NCH_2)^+$], 192 (17) [$(M\text{-}PicCH_2)^+$], 147 (20) [$(PicCH_2NC_2H_3)^+$], 133 (54) [$(PicCH_2NCH)^+$], 106 (30) [$(PicCH_2)^+$].

N,N-bis[2-(4-chloropyridyl)methyl]-N',N'-dimethylethyl-1,2-diamine (Cl-iso-BPMEN) (11): 1.10 g of 4-chloropyridine-2-carboxaldehyde (7.77 mmol) was dissolved in DCM (50 mL), 0.43 mL of N,N-dimethylethylene-1,2-diamine (3.89 mmol) added and the resultant solution stirred for 1 hour. This was added to a suspension of sodium tri(acetoxy)borohydride (2.31 g, 10.9 mmol) in DCM (50 mL) and stirred for a further 18 hours. The reaction mixture was quenched with saturated sodium hydrogen carbonate solution, the organic layer separated and the aqueous layer extracted with DCM (2×100 mL). All organic fractions were combined, dried ($MgSO_4$) and all volatiles removed to give **11** as a yellow oil (1.11 g, 84 %). ^{1}H-NMR ($CDCl_3$): δ 8.38 (d, 2H, *J*=5Hz, 6-Py*H*), 7.54 (d, 2H, *J*=2Hz, 3-Py*H*), 7.15 (dd, 2H, *J*=5 and 2Hz, 5-Py*H*), 3.84 (s, 4H, PyC*H*$_2$), 2.69 (m, 2H, PyCH$_2$NC*H*$_2$), 2.49 (m, 2H, C*H*$_2$NMe$_2$), 2.19 (s, 6H, N*Me*). ^{13}C-NMR ($CDCl_3$): δ 161.4 (*ipso*), 149.9, 144.6 (*ipso*), 123.2, 122.5, 60.4 (Py*CH*$_2$), 57.4 (N*CH*$_2$), 52.4 (N*CH*$_2$), 45.7 (N*Me*). MS (EI): *m*/*z* (%) 338 (3) [M^+], 280 (56) [$(M\text{-}Me_2NCH_2)^+$], 246 (12) [$(M\text{-}(MeN(CH_2)_2)(Cl))^+$], 212 (9) [$(M\text{-}PyCH_2)^+$], 167 (12) [$(M\text{-}(PyCH_2)(HNMe_2))^+$], 154 (34) [$(PyCH_2NCH)^+$], 126 (20) [$(PyCH_2)^+$], 58 (100) [$(Me_2NCH_2)^+$].

N,N-bis[2-(4-methoxypyridyl)methyl]-N',N'-dimethylethyl-1,2-diamine (OMe-iso-BPMEN) (12): A mixture of N,N-dimethylethylene-1,2-diamine (0.34 mL, 3.11 mmol) and 4-methoxypyridine-2-carboxaldehyde (0.98 g, 7.15 mmol) was stirred in DCM (50 mL) for 1 hour and, subsequent to this period, added to a stirring suspension of sodium tri(acetoxy)borohydride (1.98 g, 9.32 mmol) in DCM (75 mL). Upon stirring for 18 hours, the reaction was quenched using saturated sodium hydrogen carbonate solution. The organic layer was separated and the aqueous phase

extracted with DCM (2×125 mL), The organic layers were combined, dried ($MgSO_4$) and the solvent removed using the rotary evaporator to give **12** as a yellow oil (0.64 g, 63 %). ^{1}H-NMR ($CDCl_3$): δ 8.30 (d, 2H, *J*=5Hz, 6-Py*H*), 7.09 (d, 2H, *J*=2Hz, 3-Py*H*), 6.66 (dd, 4H, *J*=5 and 2Hz, 5-Py*H*), 3.82 (s, 6H, -O*Me*), 3.79 (s, 4H, PyCH_2), 2.71 (m, 2H, $PyCH_2NCH_2$), 2.53 (m, 2H, CH_2NMe_2), 2.21 (s, 6H, N*Me*). ^{13}C-NMR ($CDCl_3$): δ 166.2 (*ipso*), 162.8 (*ipso*), 150.0, 108.9, 108.5, 60.9 (PyCH_2), 56.6 (NCH_2), 55.0 (O*Me*), 51.6 (NCH_2), 45.0 (N*Me*). MS (EI): *m/z* (%) 330 (1) [M^+], 272 (27) [$(M\text{-}Me_2NCH_2)^+$], 208 (5) [$(M\text{-}PyCH_2)^+$], 181 (14), 149 (16) [$(PyCH_2NCH)^+$], 138 (11) [$(PyCH_2NH)^+$], 123 (26) [$(PyCH_3)^+$], 71 (29) [$(Me_2NC_2H_3)^+$], 58 (100) [$(Me_2NCH_2)^+$].

Synthesis of the metal complexes

[Fe(**2**)$(OTf)_2$] : A THF (20 mL) solution of **2** (0.30 g, 0.87 mmol) was added to a stirring solution of $Fe(OTf)_2(CH_3CN)_2$ (379 mg, 0.87 mmol) in THF (20 mL). The resulting light brown solution was allowed to stir overnight, upon which a yellow precipitate had formed. The volume of THF was reduced to approximately 10 mL and the mixture filtered. The yellow solid was washed three times with THF (2 mL) and once with diethyl ether (10 mL) and dried under vacuum to give a yellow powder (0.26g, 43 %). ^{1}H-NMR (CD_2Cl_2): δ 168.4 (2H, PyH_α), 129.9 (2H, H_A), 94.9 (2H, H_C), 75.9 (6H, N*Me*), 52.0 (2H, PyH_β), 51.7 (2H, Py$H_{\beta'}$), 23.9 (4H, H_B), -17.6 (2H, H_D). ^{1}H-NMR (CD_3CN, all peaks appear as broad singlets): δ 150, 89, 70, 45, 30, 25, 14. ^{19}F-NMR (CD_2Cl_2): δ -27.7 ($\nu_{1/2}$ = 540 Hz). ^{19}F-NMR (CD_3CN): δ -78.9 (95%, $\nu_{1/2}$ = 740 Hz, uncoordinated OTf^-), -22.8 (≈5 %, very broad, coordinated OTf^-). MS (FAB+): *m/z* (%) 543 ([M-OTf]$^+$). Anal. Calcd. (found) for $C_{16}H_{20}F_6FeN_6O_6S_2$: C, 31.19 (31.29); H, 2.91 (3.00); N, 8.08 (8.09). μ_{eff} (CD_3CN, 298K) = 4.42 μ_B.

[Fe(**3**)$(OTf)_2$] : The same procedure as for complex [Fe(**2**)$(OTf)_2$] gave [Fe(**3**)$(OTf)_2$] as a brown powder (67 %). ^{1}H-NMR (CD_2Cl_2): δ 167.6 (2H, PyH_α), 108.5 (2H, H_A), 104.6 (2H, H_C), 74.6 (6H, N*Me*), 47.4 (2H, PyH_β), 45.5 (2H, Py$H_{\beta'}$), 24.5 (2H, H_B), 7.4 (6H, O*Me*). ^{1}H-NMR (CD_3CN, all peaks appear as broad singlets): δ 144, 121, 80 (NMe), 43, 39, 27, 14. ^{19}F-NMR (CD_2Cl_2): δ -23.9 ($\nu_{1/2}$ = 1180 Hz). ^{19}F-NMR (CD_3CN): δ -73.7 ($\nu_{1/2}$ = 1540 Hz). MS (FAB+): *m/z* (%) 684 (30, [M]$^+$), 535 (100,

[M-OTf]$^+$). Anal. Calcd. (found) for $C_{20}H_{26}F_6FeN_4O_8S_2$: C, 35.1 (34.95); H, 3.83 (3.72); N, 8.19 (8.05). μ_{eff} (CD_3CN, 298K) = 4.76 μ_B.

[Fe(**4**)$(OTf)_2$]: The same procedure as for complex [Fe(**2**)$(OTf)_2$] gave [Fe(**4**)$(OTf)_2$] as a yellow powder (1.59 g, 78 %). ^{1}H-NMR (CD_2Cl_2): δ 164.5 (2H, H_α), 151.0 (2H, H_A), 87.3 (2H, H_C), 79.3 (6H, N*Me*), 64.3 (2H, PyH_β), 56.9 (2H, Py$H_{\beta'}$), 17.1 (2H, H_B), -31.7 (2H, PyH_D). ^{1}H-NMR (CD_3CN, all peaks appear as broad singlets): δ 17.9 (H_A), 14.8 (H_α), 12.4 (H_β, $H_{\beta'}$, H_C), 8.8 (NMe), 7.6 (H_B), 2.5 (H_D). ^{19}F-NMR (CD_2Cl_2): δ -32.8 ($\nu_{1/2}$ = 820 Hz). ^{19}F-NMR (CD_3CN): δ -77.7 ($\nu_{1/2}$ = 310 Hz, uncoordinated OTf^-), -20 (≈5 %, very broad, coordinated OTf^-). MS (FAB+): *m/z* (%) 626 ([M]$^+$), 477 ([M-OTf]$^+$). Anal. Calcd. (found) for $C_{16}H_{20}F_6FeN_6O_6S_2$: C, 30.68 (30.61); H, 3.22 (3.07); N, 13.42 (13.53). μ_{eff} (CD_2Cl_2) = 4.89 μ_B. μ_{eff} (CD_3CN) = 2.86 μ_B.

[Fe(**5**)$(OTf)_2$]: The same procedure as for complex [Fe(**2**)$(OTf)_2$] gave an off-white solid. ^{1}H-NMR (CD_2Cl_2): δ 106 (s, 2H, H_α), 60 (s, 2H, H_A), 55 (s, 2H, H_C), 46.5 (s, 2H, H_β), 55 (s, 2H, $H_{\beta'}$), 10 (s, 2H, H_γ), 7.5 (s, 2H, H_B), 3.7 (s, 2H, H_D). ^{1}H NMR (CD_3CN) δ 99.7 (s, 2H, H_α), 61.8 (s, 2H, H_C), 59.2 (s, 2H, H_A), 54.6 (s, 2H, H_β), 54.0 (s, 2H, $H_{\beta'}$), 46.0 (s, 2H, H_γ), 2.5 (2s, 4H, $H_{C,D}$). ^{19}F-NMR (CD_2Cl_2): δ -33 ($\nu_{½}$ = 560 Hz). ^{19}F NMR (CD_3CN) δ -60.3 ($\nu_{1/2}$ = 400Hz). MS (+FAB): *m/z* (%) 449 (100) [(M-OTf)$^+$]. Anal. Calcd. (found) for $C_{16}H_{16}F_6FeN_2O_8S_2$: C, 32.12 (32.04); H, 2.70 (2.79); N, 4.68 (4.59). μ_{eff} (CD_3CN) = 4.96 μ_B.

[Fe(**6**)$(OTf)_2$]: A solution of BPMES **6** (0.52 g, 1.88 mmol) in THF (10 mL) was added to a solution of $Fe(OTf)_2(CH_3CN)_2$ (0.82 g, 1.88 mmol) in THF (10 mL) and the resultant mixture was stirred overnight. The suspension was filtered and washed with diethyl ether to give an off-white powder (0.72 g, 82%). ^{1}H-NMR (CD_2Cl_2): δ 132 (s, 2H, H_α), 94 (s, 2H, H_A), 88 (s, 2H, H_C), 83 (s, 2H, H_B), 53.6 (s, 2H, H_β), 47.5 (s, 2H, $H_{\beta'}$), -5 (s, 2H, H_γ), -15 (s, 2H, H_D). ^{1}H NMR (CD_3CN) δ 40-20 (very broad), 6 (broad), 2 (broad). ^{19}F-NMR (CD_2Cl_2): δ -20.0 ($\nu_{½}$ = 2400 Hz). ^{19}F-NMR (CD_3CN): δ -76.1 ($\nu_{½}$ = 132 Hz). MS (+FAB): *m/z* (%) 481 [(M–OTf)$^+$]. Anal Calcd. (found) for $C_{16}H_{16}F_6FeN_2O_6S_4$: C, 30.49 (30.61); H, 2.56 (2.48); N, 4.44 (4.41). μ_{eff} (CD_3CN) = 2.82 μ_B.

[Fe(**7**)$(OTf)_2$]: The same procedure as for complex [Fe(**2**)$(OTf)_2$] gave a white solid. (0.37 g, 59%). ^{1}H NMR (CD_2Cl_2): δ 106.6 (s, 2H, H_α), 64.7 (s, 2H, H_A), 50.9 (s, 2H, H_β), 45.8 (s, 2H, $H_{\beta'}$), 12.3 (s, 2H, H_B), 11.7 (s, 2H, H_γ), 3.7 (s, 2H, H_C), 1.3 (s, 2H, H_C). ^{1}H NMR (CD_3CN, many signals are very broad) δ 72 (s, 2H, H_A), 52 (s, 2H, H_α), 41 (s, 2H, H_β), 38 (s, 2H, $H_{\beta'}$), 33 (s, 2H, ArH_C), 10 (s, 2H, H_γ), 2.9 (s, 2H, H_B), 2.6 (s, 2H, ArH_D). ^{19}F-NMR (CD_2Cl_2): δ -35 ($\nu_{½}$ = 750 Hz). ^{19}F NMR (CD_3CN) δ –65.6 ($\nu_{1/2}$ = 400Hz). MS (+FAB): *m/z* (%) 649 [M^+], 497 [$(M\text{-}OTf)^+$]. Anal. Calcd. (found) for $C_{20}H_{16}F_6FeN_2O_8S_2$: C, 37.17 (37.25); H, 2.50 (2.41); N, 4.33 (4.28). μ_{eff} (CD_3CN) = 5.17 μ_B.

[Fe(**8**)$(OTf)_2$]: A solution of BPMPhS **8** (0.39 g, 1.20 mmol) in THF (10 mL) was added to a solution of $Fe(OTf)_2(CH_3CN)_2$ (0.52 g, 1.20 mmol) in THF (10 mL) and the resultant mixture was stirred for one week. The THF was removed until the solution was at a minimum and the complex was precipitated out by the addition of pentane (10 mL). The precipitate was washed twice with pentane (2 x 5 mL) yielding a yellow powder (0.49 g, 60%). ^{1}H-NMR (CD_2Cl_2): δ 133.5 (s, 2H, H_α), 69.9 (s, 2H, H_A), 52.9 (s, 2H, H_β), 48.6 (s, 2H, $H_{\beta'}$), 34.4 (s, 2H, H_B), 17.6 (s, 2H, H_D), -5.3 (s, 2H, H_γ), -21.1 (s, 2H, H_C). ^{1}H NMR (CD_3CN) δ 22 (broad s, 2H, H_α), 15.5 (s, 2H, H_β), 14 (s, 2H, $H_{\beta'}$), 11.5 (s, 2H, ArH_C), 8.8 (2s, 2H, H_D), 4.8 (s, 2H, H_B), 4.3 (s, 2H, H_γ). ^{19}F-NMR (CD_2Cl_2): δ -20.6 ($\nu_{½}$ = 2900 Hz). ^{19}F-NMR (CD_3CN): δ -77.1 ($\nu_{½}$ = 450 Hz). MS (+FAB): *m/z* (%) 529 [$(M–OTf)^+$]. Anal Calcd. (found) for $C_{20}H_{16}F_6FeN_2O_6S_4$: C, 35.41 (35.50); H, 2.38 (2.47); N, 4.13 (4.20). μ_{eff} (CD_3CN) = 2.64 μ_B.

[Fe(**10**)Cl_2]: Within minutes of adding a solution of **10** (0.55 g, 1.84 mmol) in THF (25 mL) to a stirring suspension of $FeCl_2$ (0.22 g, 1.76 mmol) in THF (25 mL) an orange precipitate began to form. The stirring was continued overnight, after which the volume of THF was reduced to approximately 5 mL and the mixture filtered. The solid was washed with THF (2×5 mL) and diethyl ether (50 mL), and dried under vacuum. It was then dissolved in DCM, filtered, the DCM solution reduced in volume and pentane added to precipitate the product. Isolation of the solid by filtration and drying under vacuum gave an orange powder (0.48 g, 65.0 %). ^{1}H-NMR (CD_2Cl_2): δ 143.2 (2H, PyH_α), 89.7 (2H, H_A), 65.2 (6H, N*Me*), 48.7 (2H, PyH_β), 44.0 (2H, PyH_β), 3.2 (2H, H_B), -21.6 (6H, Py*Me*). MS (+FAB): *m/z* (%) 424 ($[M]^+$), 389

([M-Cl]$^+$). Anal. Calcd. (found) for $C_{18}H_{26}Cl_2FeN_4$: C, 50.85 (50.72); H, 6.16 (6.15); N, 13.18 (13.03). μ_{eff} (CD_2Cl_2) = 5.07 μ_B.

[Fe(**10**)(OTf)$_2$]: A combination of 1 equivalent of [Fe(**10**)Cl$_2$] (0.45 g, 1.06 mmol) and 2 equivalents of silver(I) triflate (0.55 g, 2.13 mmol) was stirred in DCM (50 mL), overnight. Subsequently, the mixture was filtered through celite to remove silver(I) salts and the celite washed with DCM. The filtrate and washings were combined and concentrated to a volume of approximately 10 mL and pentane added to precipitate the product. After filtration the solid was dried under vacuum to give a yellow powder (0.60 g, 86.3 %). ^{1}H-NMR (CD_2Cl_2): δ 134.9 (2H, PyH_α), 118.9 (2H, H_A), 104.8 (6H, N*Me*), 56.7 (1H, H_C), 51.9 (1H, H_D), 46.2 (2H, PyH_β), 45.7 (2H, PyH_β), 2.8 (2H, H_B), -7.9 (6H, Py*Me*). ^{1}H-NMR (CD_3CN): δ 118.9 (2H, PyH_α), 101.1 (6H, N*Me*), 98.6 (2H, H_A), 52.2 (2H, PyH_β), 49.9 (1H, H_C), 46.5 (2H, PyH_β), 45.1 (1H, H_D), 9.0 (6H, Py*Me*), 6.1 (2H, H_B). ^{19}F-NMR (CD_2Cl_2): δ -28.0 ($\nu_{1/2}$ = 610Hz). ^{19}F-NMR (CD_3CN): δ -69.2 ($\nu_{1/2}$ = 410Hz). MS (+FAB): *m/z* (%) 503 ([M-OTf]$^+$). Anal. Calcd. (found) for $C_{20}H_{26}F_6FeN_4O_6S_2$: C, 36.82 (36.71); H, 4.02 (3.95); N, 8.59 (8.45). μ_{eff} (CD_2Cl_2) = 4.95 μ_B. μ_{eff} (CD_3CN) = 4.79 μ_B.

[Fe(**11**)Cl$_2$]: Addition of a solution of **11** (1.35 g, 3.98 mmol) in THF (50 mL) to a suspension of $FeCl_2$ (0.45 g, 3.58 mmol) in THF (50 mL), followed by stirring overnight led to the formation of a red precipitate. The volume of THF was reduced to approximately 10 mL, the mixture filtered, and the solid obtained washed with THF (3×10 mL). It was then dissolved in DCM, the solution filtered, reduced in volume and pentane added to precipitate the product. Drying of the solid under vacuum gave a red powder (1.46 g, 87.2 %). ^{1}H-NMR (d$_6$-DMSO): δ 149.1 (2H, PyH_α), 99.8 (2H, H_A), 77.8 (6H, N*Me*), 47.3 (2H, PyH_β), 46.4 (2H, PyH_β), 0.0 (2H, H_B). MS (+FAB): *m/z* (%) 895 ([2M-Cl]$^+$), 466 ([M]$^+$), 429 ([M-Cl]$^+$). Anal. Calcd. (found) for $C_{16}H_{20}Cl_4FeN_4$: C, 41.24 (41.06); H, 4.33 (4.23); N, 12.02 (11.92). μ_{eff} (CD_2Cl_2) = 5.28 μ_B.

[Fe(**11**)(OTf)$_2$]: A mixture of [Fe(**11**)Cl$_2$] (1.22 g, 2.61 mmol) and 2 equivalents of silver(I) triflate (1.34 g, 5.22 mmol) were stirred in DCM (100 mL) overnight. It was, subsequently, filtered through celite and the celite washed with copious amounts of

DCM. The filtrates were combined, reduced in volume to approximately 5 mL and filtered to separate soluble impurities from the solid product. Drying under vacuum gave a yellow powder (0.72 g, 40.0 %). ^{1}H-NMR (CD_2Cl_2): δ 149.2 (2H, PyH_α), 115.8 (2H, H_A), 101.1 (6H, N*Me*), 46.2 (2H, PyH_β), 45.3 (2H, PyH_β). ^{1}H-NMR (CD_3CN): δ 109.6 (2H, PyH_α), 103.0 (8H, N*Me* and H_A), 49.4 (2H, PyH_β), 46.3 (1H, H_C), 43.4 (4H, PyH_β and H_D), 10.5 (2H, H_B). ^{19}F-NMR (CD_2Cl_2): δ -25.8 ($\nu_{1/2}$ = 1740Hz). ^{19}F-NMR (CD_3CN): δ -64.1 ($\nu_{1/2}$ = 1130Hz). MS (+FAB): *m/z* (%) 693 ($[M]^+$), 543 ($[M\text{-}OTf]^+$). Anal. Calcd. (found) for $C_{18}H_{20}Cl_2F_6FeN_4O_6S_2$: C, 31.19 (31.01); H, 2.91 (2.80); N, 8.08 (7.99). μ_{eff} (CD_2Cl_2) = 5.10 μ_B. μ_{eff} (CD_3CN) = 4.85 μ_B.

[Fe(**12**)$(OTf)_2$]: The ligand **12** (0.52 g, 1.57 mmol) was dissolved in THF (75 mL) was added slowly to a stirring solution of $Fe(OTf)_2(CH_3CN)_2$ (0.62 g, 1.42 mmol), in THF (75 mL), and allowed to continue stirring overnight during which time a white precipitate formed. Subsequently, the volume of THF was reduced to approximately 10 mL and the mixture filtered. The solid obtained was washed twice with THF (10 mL), once with diethyl ether (50 mL) and dried under vacuum to give a white powder (0.59 g, 60.8 %). ^{1}H-NMR (CD_2Cl_2): δ 129.4 (2H, PyH_α), 122.1 (2H, H_A), 111.4 (6H, N*Me*), 54.7 (2H, H_C and H_D), 46.2 (2H, PyH_β), 43.8 (2H, PyH_β), 13.5 (2H, H_B), 4.42 (6H, O*Me*). ^{1}H-NMR (CD_3CN): δ 130.1 (2H, PyH_α), 101.7 (8H, N*Me* and H_A), 54.4 (2H, PyH_β), 49.0 (2H, H_C and H_D), 45.1 (2H, PyH_β), 5.2 (6H, O*Me*), 4.8 (2H, H_B). ^{19}F-NMR (CD_2Cl_2): δ -26.5 ($\nu_{1/2}$ = 980Hz). ^{19}F-NMR (CD_3CN): δ -71.5 ($\nu_{1/2}$ = 280Hz). MS (+FAB): *m/z* (%) 684 ($[M]^+$), 535 ($[M\text{-}OTf]^+$). Anal. Calcd. (found) for $C_{20}H_{26}F_6FeN_4O_8S_2$: C, 35.10 (34.98); H, 3.83 (3.72); N, 8.19 (8.06). μ_{eff} (CD_2Cl_2) = 5.07 μ_B. μ_{eff} (CD_3CN) = 4.80 μ_B.

Crystallographic Details

Table 6 provides a summary of the crystallographic data for compounds [Fe(**6**)$(OTf)_2$] and [Fe(**7**)$(OTf)_2$]. Data were collected using Oxford Diffraction Xcalibur 3 ([Fe(**6**)$(OTf)_2$]) and Xcalibur PX Ultra ([Fe(**7**)$(OTf)_2$]) diffractometers. The structure of [Fe(**6**)$(OTf)_2$] was found to be a racemic twin [R_1^+ = 0.0627, R_1^- = 0.0628; x^+ = 0.49(4), x^- = 0.51(4)]. Other issues with the structure of [Fe(**6**)$(OTf)_2$],

pertaining to the choice of space group, are covered in the supporting information. CCDC 685212 and 685213, respectively.

Table 6. Crystallographic Data for compounds [Fe(**6**)OTf_2] and [Fe(**7**)OTf_2].

data	[Fe(**6**)OTf_2]	[Fe(**7**)OTf_2]
chemical formula	$C_{16}H_{16}F_6FeN_2O_6S_4$	$C_{20}H_{16}F_6FeN_2O_8S_2$
solvent	—	—
fw	630.40	646.32
T (°C)	–100	–100
space group	C2 (no. 5)	$P2_1/n$ (no. 14)
a (Å)	8.2056(2)	10.87027(8)
b (Å)	15.9411(5)	20.82017(13)
c (Å)	18.1132(5)	11.23438(10)
β (deg)	102.141(3)	109.0983(9)
V (Å^3)	2316.33(11)	2402.65(3)
Z	4 [a]	4
ρ_{calcd} (g cm^{-3})	1.808	1.787
λ (Å)	0.71073	1.54184
μ (mm^{-1})	1.097	7.577
measured reflns	17222	34120
unique reflns	7397	4640
R(int)	0.037	0.034
observed reflns	7053	3910
R_1 [b]	0.061	0.027
wR_2 [c]	0.145	0.074

[a] There are two crystallographically independent C_2 symmetric molecules. [b] $R_1 = \Sigma||F_o| - |F_c||/\Sigma|F_o|$. [c] $wR_2 = \{\Sigma[w(F_o^2 - F_c^2)^2] / \Sigma[w(F_o^2)^2]\}^{1/2}$; $w^{-1} = \sigma^2(F_o^2) + (aP)^2 + bP$.

Acknowledgements

We are grateful to EPSRC and BP Chemicals Ltd. for a CASE Award for J.E. We thank Mr. Richard Sheppard and Mr. Peter Haycock for their assistance in NMR measurements.

Supporting Information Available:

The supporting information includes experimental details, NMR spectra and crystallographic details. This information can be obtained free of charge via the Internet at http://pubs.acs.org.

References

1 R. A. Sheldon and J. K. Kochi, 'Metal-catalysed oxidations of organic compounds', Academic Press, 1981.
2 A. E. Shilov and G. B. Shul'pin, 'Activation of catalytic reactions of saturated hydrocarbons in the presence of metal complexes', Kluwer, 2000.
3 J. A. Labinger, *J. Mol. Catal.*, 2004, **220**, 27.
4 S. S. Stahl, J. A. Labinger, and J. E. Bercaw, *Angew. Chem. Int. Ed. Engl.*, 1998, **37**, 2180.
5 W. Partenheimer, *Catal. Today*, 1995, **23**, 69.
6 B. Meunier, S. P. de Visser, and S. Shaik, *Chem. Rev.*, 2004, **104**, 3947.
7 B. Meunier, *Chem. Rev.*, 1992, **92**, 1411.
8 I. V. Kozhevnikov, in 'Catalysis by Polyoxometalates', Chichester, 2002.
9 C. L. Hill and C. M. Prosser-McCartha, *Coord. Chem. Rev.*, 1995, **143**, 407.
10 N. Mizuno and M. Misono, *Chem. Rev.*, 1998, **98**, 199.
11 L. Que Jr. and W. B. Tolman, *Nature*, 2008, **455**, 333.
12 S. Tanase and E. Bouwman, *Adv. Inorg. Chem.*, 2006, **58**, 29.
13 M. Costas, K. Chen, and L. Que Jr., *Coord. Chem. Rev.*, 2000, **200-202**, 517.
14 B. Meunier, in 'Biomimetic Oxidations Catalyzed by Transition Metal Complexes', London, 2000.
15 M. M. Abu-Omar, A. Loalza, and N. Hontzeas, *Chem. Rev.*, 2005, **105**, 2227.
16 M. Costas, M. P. Mehn, M. P. Jensen, and L. Que Jr., *Chem. Rev.*, 2004, **104**, 939.
17 S. V. Kryatov, E. V. Rybak-Akimova, and S. Schindler, *Chem. Rev.*, 2005, **105**, 2175.
18 R. H. Holm and J. P. Donahue, *Polyhedron*, 1993, **12**, 571.
19 C. W. Jones, 'Applications of Hydrogen Peroxide and Derivatives', The Royal Society of Chemistry, 1999.
20 C. L. Hill, *Nature*, 1999, **401**, 436.
21 C. Walling, *Acc. Chem. Res.*, 1975, **8**, 125.
22 J. Kim, R. G. Harrison, C. Kim, and L. Que Jr., *J. Am. Chem. Soc.*, 1996, **118**, 4373.
23 M. H. Lim, J.-U. Rohde, A. Stubna, M. R. Bukowski, M. Costas, R. Y. N. Ho, E. Münck, W. Nam, and L. Que Jr., *PNAS*, 2003, **100**, 3665.

24 G. J. P. Britovsek, J. England, and A. J. P. White, *Inorg. Chem.*, 2005, **44**, 8125.

25 K. Chen and L. Que Jr., *Chem. Commun.*, 1999, 1375.

26 J. England, G. J. P. Britovsek, N. Rabadia, and A. J. P. White, *Inorg. Chem.*, 2007, **46**, 3752.

27 M. S. Chen and M. C. White, *Science*, 2007, **318**, 783.

28 A. Company, L. Gómez, M. Güell, X. Ribas, J. M. Luis, L. Que Jr., and M. Costas, *J. Am. Chem. Soc.*, 2007, **129**, 15766.

29 A. Company, L. Gómez, X. Fontrodona, X. Ribas, and M. Costas, *Chem. Eur. J.*, 2008, **14**, 5727.

30 K. Chen and L. Que Jr., *J. Am. Chem. Soc.*, 2001, **123**, 6327.

31 K. Chen, M. Costas, and L. Que Jr., *Dalton Trans.*, 2002, 672.

32 A. Bassan, M. R. A. Blomberg, P. E. M. Siegbahn, and L. Que Jr., *Chem. Eur. J.*, 2005, **11**, 692.

33 W. Nam, *Acc. Chem. Res.*, 2007, **40**, 522.

34 L. Que Jr., *Acc. Chem. Res.*, 2007, **40**, 493.

35 J. T. Groves, *J. Chem. Educ.*, 1985, **62**, 928.

36 E. Klinker, J., J. Kaizer, W. W. Brennessel, N. L. Woodrum, C. J. Cramer, and L. Que Jr., *Angew. Chem. Int. Ed.*, 2005, **44**, 3690.

37 J.-U. Rohde, J.-H. In, M. H. Lim, W. W. Brennessel, M. R. Bukowski, A. Stubna, E. Münck, W. Nam, and L. Que Jr., *Science*, 2003, **299**, 1037.

38 A. Thibon, J. England, M. Martinho, V. G. Young Jr., J. R. Frisch, R. Guillot, J.-J. Girerd, E. Münck, L. Que Jr., and F. Banse, *Angew. Chem. Int. Ed.*, 2008, **47**, 7064.

39 F. Tiago de Oliveira, A. Chanda, D. Banerjee, X. Shan, S. Mondal, L. Que Jr., E. L. Bominaar, E. Münck, and T. J. Collins, *Science*, 2007, **315**, 835.

40 K. Chen, M. Costas, J. Kim, A. Tipton, and L. Que Jr., *J. Am. Chem. Soc.*, 2002, **124**, 3026.

41 M. Costas and L. Que Jr., *Angew. Chem. Int. Ed.*, 2002, **41**, 2179.

42 Y. Hitomi, S. Furukawa, M. Higuchi, T. Shishido, and T. Tanaka, *J. Mol. Catal. A: Chem.*, 2008, **288**, 83.

43 G. J. P. Britovsek, J. England, and A. J. P. White, *Dalton Trans.*, 2006, 1399.

44 J. England, C. R. Davis, M. Banaru, A. J. P. White, and G. J. P. Britovsek, *Adv. Synth. Catal.*, 2008, **350**, 883.

45 C. Hemmert, M. Renz, H. Gornitzka, S. Soulet, and B. Meunier, *Chem. Eur. J.*, 1999, **5**, 1766.

46 M. Renz, C. Hemmert, B. Donnadieu, and B. Meunier, *Chem. Commun.*, 1998, 1635.

47 Y. Mekmouche, S. Ménage, C. Toia-Duboc, M. Fontecave, J.-B. Galey, C. Lebrun, and J. Pécaut, *Angew. Chem. Int. Ed.*, 2001, **40**, 949.

48 I. D. Cunningham, T. N. Danks, J. N. Hay, I. Hamerton, and S. Gunathilagan, *Tetrahedron*, 2001, **57**, 6847.

49 I. D. Cunningham, T. N. Danks, J. N. Hay, I. Hamerton, S. Gunathilagan, and C. Janczak, *J. Mol. Catal.*, 2002, **185**, 25.

50 A. C. Serra, E. C. Marçalo, and A. M. d. A. Rocha Gonsalves, *J. Mol. Catal.*, 2004, **215**, 17.

51 N. A. Stephenson and A. T. Bell, *J. Am. Chem. Soc.*, 2005, **127**, 8635.

52 Nagababu, E. and J. M. Rifkind, *Antioxidants & Redox Signaling*, 2004, **6**, 967.

53 P. Mialane, L. Tchertanov, F. Banse, J. Sainton, and J.-J. Girerd, *Inorg. Chem.*, 2000, **39**, 2440.

54 M. Delroisse, A. Rabion, F. Chardac, D. Tétard, J.-B. Verlhac, L. Fraisse, and J.-L. Séris, *J. Chem. Soc. Chem. Commun.*, 1995, 949.

55 P. A. Goodson, A. R. Oki, J. Glerup, and D. J. Hodgson, *J. Am. Chem. Soc.*, 1990, **112**, 6248.

56 C. M. Hartshorn and P. J. Steel, *J. Chem. Soc., Dalton Trans.*, 1998, 3927.

57 S. E. Livingstone and J. D. Nolan, *Aust. J. Chem.*, 1970, **23**, 1553.

58 R. Mas-Ballesté, M. Costas, T. van den Berg, and L. Que Jr., *Chem. Eur. J.*, 2006, **12**, 7489.

59 A. L. Gavrilova and B. Bosnich, *Chem. Rev.*, 2004, **104**, 349.

60 Y. Mekmouche, S. Ménage, J. Pécaut, C. Lebrun, L. Reilly, V. Schuenemann, A. Trautwein, and M. Fontecave, *Eur. J. Inorg. Chem.*, 2004, 3163.

61 N. Raffard, V. Balland, A. J. Simaan, S. Létard, M. Nierlich, K. Miki, F. Banse, E. Anxolabéhère-Mallart, and J.-J. Girerd, *C. R. Acad. Sci. (Paris) Ser. C*, 2002, **5**, 99.

62 B. Rieger, A. S. Abu-Surrah, R. Fawzi, and M. Steiman, *J. Organomet. Chem.*, 1995, **497**, 73.

63 J. Simaan, S. Poussereau, G. Blondin, J.-J. Girerd, D. Defaye, C. Philouze, J. Guilhem, and L. Tchertanov, *Inorg. Chim. Acta*, 2000, **299**, 221.

64 M. C. White, A. G. Doyle, and E. N. Jacobsen, *J. Am. Chem. Soc.*, 2001, **123**, 7194.

65 B. Adhikary, S. Liu, and C. R. Lucas, *Inorg. Chem.*, 1993, **32**, 5957.

66 H. Nekola, D. Wang, C. Grüning, J. Gätjens, A. Behrens, and D. Rehder, *Inorg. Chem.*, 2002, **41**, 2379.

67 B. M. Schmiege, M. J. Carney, B. L. Small, D. L. Gerlach, and J. A. Halfen, *Dalton Trans.*, 2007, 2547.

68 M. A. Halcrow, *Polyhedron*, 2007, **26**, 3523.

69 K. P. Bryliakov, E. A. Duban, and E. P. Talsi, *Eur. J. Inorg. Chem.*, 2005, 72.

70 H. Börzel, P. Comba, K. S. Hagen, Y. D. Lampeka, A. Lienke, G. Linti, M. Merz, H. Pritzkow, and L. V. Tsymbal, *Inorg. Chim. Acta*, 2002, **337**, 407.

71 V. Balland, F. Banse, E. Anxolabéhère-Mallart, M. Nierlich, and J.-J. Girerd, *Eur. J. Inorg. Chem.*, 2003, 2529.

72 A. S. Borovik, V. Papaefthymiou, L. F. Taylor, O. P. Anderson, and L. Que Jr., *J. Am. Chem. Soc.*, 1989, **111**, 6183.

73 H. Toftlund, *Coord. Chem. Rev.*, 1989, **94**, 67.

74 A. Fischer, W. J. Galloway, and J. Vaughan, *J. Chem. Soc.*, 1964, 3591.

75 R. W. Balk, D. J. Stufkens, R. J. Crutchley, and A. B. P. Lever, *Inorg. Chim. Acta*, 1982, **64**, L49.

76 P. Gütlich, Y. Garcia, and H. A. Goodwin, *Chem. Soc. Rev.*, 2000, **29**, 419.

77 H. Toftlund and J. J. McGarvey, *Top. Curr. Chem.*, 2004, **233**, 151.

78 H. Toftlund, *Monatsh. Chem.*, 2001, **132**, 1269.

79 K. S. Hagen, *Inorg. Chem.*, 2000, **39**, 5867.

List of Figures

Figure 9c. UV-vis spectra of $[Fe(L)(CH_3CN)_2]^{2+}$ complexes containing iso-BPMEN ligands **9**-**12** (0.5 mM, CH_3CN, 298K).

Figure 10a. The magnetic moments of iron(II) complexes containing ligands **1** – **4** in CD_3CN solution as a function of temperature.

Figure 10b. The magnetic moments of iron(II) complexes containing ligands **5** – **8**, together with complex [Fe(**1**)$(OTf)_2$] for comparison, in CD_3CN solution as a function of temperature.

Figure 10c. The magnetic moments of iron(II) complexes containing ligands **9** – **12** in CD_3CN solution as a function of temperature.

Figure 11. Product composition at various amounts of H_2O_2 in the oxidation of cyclohexane catalyzed by [Fe(**2**)$(OTf)_2$] (top), [Fe(**3**)$(OTf)_2$] (middle) and [Fe(**4**)$(OTf)_2$] (bottom). The dashed line represents the total number of equivalents of oxidised product that can be obtained.

Figure 12. Conversion of H_2O_2 into oxygenated products (A+2K curves) for different catalysts. The dashed line represents the total number of equivalents of oxidised product that can be obtained.

Graphical Abstract

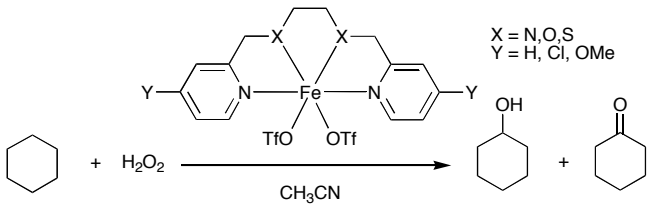

A series of non-heme iron(II) bis(triflate) complexes containing linear and tripodal tetradentate ligands has been prepared and the effect of electron withdrawing and donating substituents in the *para* position of the pyridine ligands, as well the effect of pyrazine *versus* pyridine and sulphur or oxygen donors instead of nitrogen donors on their catalytic alkane oxidation activity has been investigated.